

On the uncertainties in stone armor stability

Scaravaglione, Giulio; Melby, Jeffrey A.; Tomasicchio, Giuseppe R.; van Gent, Marcel R.A.; Saponieri, Alessandra

DOI

[10.1016/j.coastaleng.2025.104790](https://doi.org/10.1016/j.coastaleng.2025.104790)

Publication date

2025

Document Version

Final published version

Published in

Coastal Engineering

Citation (APA)

Scaravaglione, G., Melby, J. A., Tomasicchio, G. R., van Gent, M. R. A., & Saponieri, A. (2025). On the uncertainties in stone armor stability. *Coastal Engineering*, 202, Article 104790. <https://doi.org/10.1016/j.coastaleng.2025.104790>

Important note

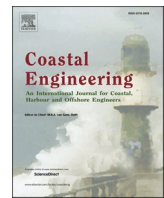
To cite this publication, please use the final published version (if applicable). Please check the document version above.

Copyright


Other than for strictly personal use, it is not permitted to download, forward or distribute the text or part of it, without the consent of the author(s) and/or copyright holder(s), unless the work is under an open content license such as Creative Commons.

Takedown policy

Please contact us and provide details if you believe this document breaches copyrights. We will remove access to the work immediately and investigate your claim.



On the uncertainties in stone armor stability

Giulio Scaravaglione^{a,1,*} , Jeffrey A. Melby^{b,1}, Giuseppe R. Tomasicchio^{c,1},
Marcel R.A. van Gent^{d,1}, Alessandra Saponieri^{c,1}

^a Department of Civil, Environmental, Land, Building Engineering and Chemistry (DICATECh), Polytechnic University of Bari, Bari, Italy

^b Coastal Structures Group, Coastal and Hydraulic Laboratory, U.S Army Engineer Research and Development Center, USA

^c Department of Engineering for Innovation, University of Salento, Lecce, Italy

^d Department of Hydraulic Engineering, Delft University of Technology and Deltares, Delft, the Netherlands

ARTICLE INFO

Keywords:

Armor stone stability
Homogeneous database
Uncertainty
Shallowness conditions
Damage

ABSTRACT

The present research aims to investigate the uncertainties in the evaluation of stone armor stability. Data synthesis was achieved by collecting and homogenizing data from 4 distinct studies, considering the inherent variability of the original data. Established stability equations are then applied to the synthesized database to assess both the strengths and limitations of different approaches across deep, shallow, and very shallow water. The results indicate that while nearly all formulations perform well in deep water, some inadequacies emerge in shallow and very shallow water. To address these limitations, the stability equations were recalibrated using the new database, with a focus on error and uncertainty quantification. The refitted Etamad-Shahidi et al. (ES, 2020) and Modified ES (Scaravaglione et al., 2025) equations consistently demonstrate better predictive capability across all water depths. However, damage assessment reveals persistent uncertainties across all formulations, rendering the selection of a single equation inconclusive, mainly due to the high uncertainty of the available laboratory data. Further synthesizing and homogenizing require additional modeling given the varying modeling approaches, the non-homogenous nature of the parametric data, and the limited understanding possible of the detailed laboratory techniques and data analysis carried out.

1. Introduction

Stone-armored rubble mound structures are among the most common, effective, and widely adopted solutions in harbor construction and coastal defense against waves and currents, and coastal flooding in general. Fig. 1 reports a schematic cross-section of a standard stone-armored rubble mound breakwater together with the main variables and geometrical notations used in the present study.

Estimating hydraulic stability for armor stone layers is commonly based on the application of stability formulae found in design manuals (e.g., the Coastal Engineering Manual (USACE, 2002) and the Rock

Manual (CIRIA/CUR/CETMEF, 2007)), which are semi-empirical based. These equations are predominantly derived from datasets obtained through small-scale physical model experiments conducted at different coastal laboratories worldwide or by employing numerical modeling and machine-learning techniques, or some hybridization of these methods. Armor damage may be influenced by numerous uncertainties. In recent decades, while new relationships have been introduced to broaden the applicability of the design equations, limited progress has been made to quantify and reduce equation uncertainty. A distinction is generally made between intrinsic (or aleatory) and epistemic uncertainty. The former is irreducible and associated with the random

* Corresponding author.

E-mail address: giulio.scaravaglione@poliba.it (G. Scaravaglione).

¹ All authors contributed in equal measure to all stages of the development and production of this paper. All authors have read and agreed to the published version of the manuscript.

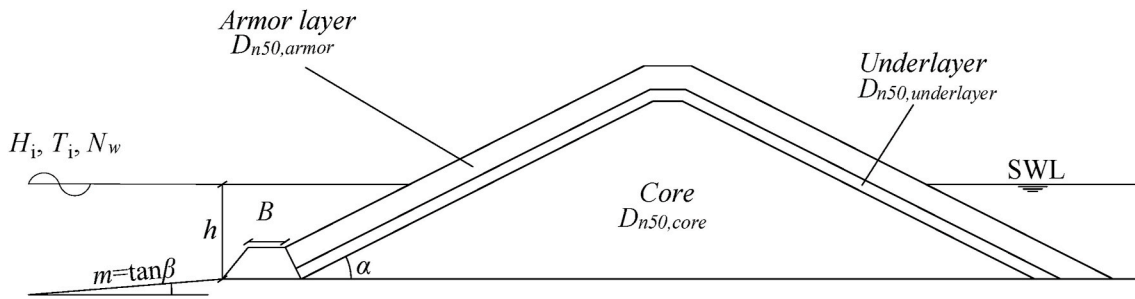


Fig. 1. Schematic cross-section of a standard stone-armored breakwater.

occurrence of processes in time and space. The latter concerns the current knowledge about processes, observations, and methods and is, in theory, reducible with appropriate precautions (Kroon et al., 2020). The effects of intrinsic uncertainty on hydraulic stability have been often assumed dominant over epistemic uncertainty due to the inherent challenges in isolating their respective contributions (Losada, 2021). However, the magnitude of both contributions has not yet been explicitly quantified to validate this assumption. Therefore, it remains a major knowledge gap in the probabilistic design of coastal structures, posing an impediment to understanding related risks.

Moreover, the adaptation of rubble mound breakwaters is becoming increasingly critical in the face of climate change, as rising sea levels and heightened storm activity expose coastal structures to more intense wave attacks. Higher sea levels and the increased frequency of extreme events will enhance the risk of structural damage and its consequences, such as impacts to harbor activities and navigation and flooding of the hinterland. However, incorporating the effects of climate change into the design of coastal structures is challenging due to the significant uncertainties inherent in climate change scenarios and sea level rise projections (Mares-Nasarre et al., 2024). There is a growing need to address these uncertainties and design with accurate reliability more cost-effective, resource-efficient, and spatially economical structures, rather than accounting for all possible uncertainties by overdesigning the structures.

Recently, significant progress has been achieved, although more details of the sources of uncertainties in stability and damage formulae are warranted.

Early relations to assess the hydraulic stability of armor stones were developed by e.g., Iribarren (1938), Hudson (1959), Losada and Gimenez-Curto (1979). Considerable progress was made by Thompson and Shuttler (1975), hereafter referred to as TS, who recognized the importance of wave breaking, rock placement, and the number of waves in evaluating the hydraulic stability of a rubble mound structure. The TS dataset (135 data) used in the present study is provided in Verhagen and Mertens (2009) and can be accessed via the open-access link: <https://resolver.tudelft.nl>.

The dataset of TS was reanalyzed by van der Meer (1988) and van der Meer (2021), hereafter referred to as VDM, who performed a comprehensive laboratory experimental campaign and quantified the influence of some additional parameters on the hydraulic stability of stone armor layers. Two distinct formulae for plunging (Eq. (1a)) and surging (Eq. (1b)) waves were derived and widely utilized in design practice and research, primarily limited to deep water and non-sloping conditions:

$$\frac{H_s}{\Delta D_{n50}} = 6.49 c_{pl} P^{0.18} \left(\frac{S}{\sqrt{N_w}} \right)^{0.2} \xi_{s-1,0}^{-0.5} \quad \text{Eq. (1a)}$$

if $\xi_{s-1,0} \leq \xi_{s-1,0,c}$ and/or $\cot \alpha \geq 4$

$$\frac{H_s}{\Delta D_{n50}} = 0.97 c_{su} P^{0.13} \left(\frac{S}{\sqrt{N_w}} \right)^{0.2} \sqrt{\cot \alpha} \xi_{s-1,0}^P \quad \text{Eq. (1b)}$$

if $\xi_{s-1,0} > \xi_{s-1,0,c}$

where:

N_s	stability number
$H_s = H_{1/3}$	significant wave height in the time domain
$\Delta = \rho_r / \rho_w - 1$	relative buoyant density of the armor stone
ρ_r	density of stone
ρ_w	density of water
$D_{n50} = (M_{50} / \rho_r)^{1/3}$	nominal median stone size
M_{50}	median mass of the stone grading
α	structure seaward slope angle
$S = A_e / D_{n50}^2$	damage level
A_e	average eroded area
P	notional permeability factor
g	gravity acceleration
N_w	number of waves in a storm duration
$\xi_{s-1,0} = \tan \alpha / \sqrt{2\pi H_s / g T_{m-1,0}^2}$	surf similarity parameter
$T_{m-1,0}$	negative first moment spectral wave period
$\xi_{s-1,0,c} = \left(\frac{6.49 c_{pl} P^{0.31} \sqrt{\tan \alpha}}{0.97 c_{su}} \right)^{\frac{1}{P+0.5}}$	critical surf similarity parameter
c_{pl}, c_{su}	shape coefficients

For slopes more gentle than $\cot \alpha = 4$, it is advised to use Eq. (1a), regardless of the value of the surf similarity parameter. Van der Meer (2021) gave the applicability area of the Rewritten VDM formula in a combined stability versus surf similarity parameter (SSP) graph. Shape coefficients equal to 1 means that the formulae are equal, smaller and larger values show less and better stability, respectively. The VDM dataset (294 data) used in the present study is provided in van der Meer (2021) and is available at the open-access link zenodo.org. Combined, the TS and VDM studies encompass a total of 429 data, primarily focusing on cases without a sloping foreshore or depth-induced wave breaking, although a limited number of tests were performed on a foreshore with a 1V:30H slope. TS investigated 4 impermeable structures with slope angles of 1V:2H, 1V:3H, 1V:4H and 1V:6H. In comparison, VDM investigated 4 impermeable structures with slope angles of 1V:2H, 1V:3H, 1V:4H and 1V:6H, 3 permeable structures with slope angles of 1V:1.5H, 1V:2H and 1V:3H, and 1 homogenous structure with a slope angle of 1V:2H. Recently, van der Meer et al. (2024) tested the application of the Rewritten VDM formula in shallow water. They concluded that the Rewritten VDM formula is valid much further into the shallow water region than what the Rock Manual recommends and at least to $h/H_{m0,deep} > 1.5$ (where h is the water depth at the structure toe and $H_{m0,deep}$ is the spectral wave height in deep water) and suggest the use of H_{m0} instead of H_s to better describe nonlinear waves. For shallow water with $h/H_{m0,deep} < 1.5$, no systematic trend with the energy period

($T_{m-1,0}$) is observed anymore and constant combined stability numbers are given for guidance in preliminary design.

Smith et al. (2002) conducted small-scale laboratory experiments to investigate the effects of shallow water conditions. According to the water depth classification of van Gent (1999, 2001), based on the ratio between the deep water wave height $H_{m0,deep}$ and the local water depth h , namely the relative depth ($h_r = H_{m0,deep}/h$), different water depth conditions can be established, ranging from deep (where wave breaking on the foreshore is absent) to extremely shallow foreshores (experiencing a high degree of wave breaking on the foreshore). Specifically, foreshores can be classified as deep ($h_r < 0.40$), intermediate ($0.40 < h_r < 0.75$), shallow ($0.75 < h_r < 1.50$), very shallow ($1.50 < h_r < 3$), and extremely shallow ($h_r > 3$). The work by Smith et al. (2002) was further extended by van Gent et al. (2003), hereafter referred to as VSK. The authors provided additional data on different structures and foreshore slopes. Similar to van der Meer (1988), equations for plunging (Eq. (2a)) and surging (Eq. (2b)) waves were derived, leading to a Modified van der Meer formula, adapted for shallow water:

$$\frac{H_s}{\Delta D_{n50}} = 8.4 C_{pl} P^{0.18} \left(\frac{S}{\sqrt{N_w}} \right)^{0.2} \xi_{s-1,0}^{-0.5} \left(\frac{H_{2\%}}{H_s} \right)^{-1} \quad \text{Eq. (2a)}$$

if $\xi_{s-1,0} \leq \xi_{s-1,0,c}$ and/or $\cot\alpha \geq 4$

$$\frac{H_s}{\Delta D_{n50}} = 1.3 C_{su} P^{-0.13} \left(\frac{S}{\sqrt{N_w}} \right)^{0.2} \cot\alpha^{0.5} \xi_{s-1,0}^P \left(\frac{H_{2\%}}{H_s} \right)^{-1} \quad \text{Eq. (2b)}$$

if $\xi_{s-1,0} > \xi_{s-1,0,c}$

where $H_{2\%}$ is the wave height exceeded by 2 percent of the waves that reach the structure. For slopes more gentle than $\cot\alpha = 4$, it is advised to use Eq. (2a), irrespective of the value of the surf similarity parameter. The data used in the present study are provided at the open access link 'Data Stability of rock slopes with shallow foreshores'. The work includes 207 data with 2 foreshore slopes of 1V:100H and 1V:30H, 2 structures with slope angles of 1V:2H and 1V:4H and each of them with a permeable and an impermeable core. Tests were performed for shallow water and in a few cases for very shallow water with $h_r < 3$.

In van Gent et al. (2003) and van Gent (2004), an alternative stability formula, referred to as the Simple van Gent formula (Eq. (3)) was proposed, independent from wave period or P , but including both armor (D_{n50}) and core ($D_{n50,core}$) stone nominal sizes, respectively.

$$\frac{H_s}{\Delta D_{n50}} = 1.75 \sqrt{\cot\alpha} \left(1 + \frac{D_{n50,core}}{D_{n50}} \right) \left(\frac{S}{\sqrt{N_w}} \right)^{\frac{1}{5}} \quad \text{Eq. (3)}$$

Melby and Hughes (2003) and later Melby and Kobayashi (2011), hereafter referred to as MK, developed a stability formula based on the maximum wave momentum flux, demonstrating the role of water depth for evaluating stability for both plunging (Eq. (4a)) and surging (Eq. (4b)) waves:

$$N_m = 5.0 P^{0.18} \sqrt{\cot\alpha} \left(\frac{S}{\sqrt{N_w}} \right)^{0.2} \quad \text{plunge if } s_m \geq s_{m,c} \quad \text{Eq. (4a)}$$

$$N_m = 5.0 P^{0.18} \cot\alpha^{0.5-P} \left(\frac{S}{\sqrt{N_w}} \right)^{0.2} s_m^{-P/3} \quad \text{surge if } s_m < s_{m,c} \quad \text{Eq. (4b)}$$

where $N_m = \left(\frac{M_f}{\rho_w g h^2 \Delta} \right)^{1/2} \frac{h}{D_{n50}}$ is the stability number dependent on the local water depth (h) and the nonlinear maximum wave momentum flux (M_f)_{max at the structure toe. s_m represents the wave steepness at the toe of the structure using the mean wave period (T_m) and the spectral wave height (H_{m0}). The range of applicability depends on the critical wave steepness $s_{m,c} = \cot\alpha^{-3}$, as it denotes the analytical intersection between the two equations. The formula, calibrated using the VDM data, involves}

a nonlinear wave momentum flux using a numerical Fourier solution approximated by Hughes (2004) with the following relations (Eqs. (5a,b,c)):

$$\frac{(M_f)_{max}}{\rho_w g h^2} = A_0 \left(\frac{h}{g T_m^2} \right)^{-A_1} \quad \text{Eq. (5a)}$$

$$A_0 = 0.639 \left(\frac{H_{m0}}{h} \right)^{2.026} \quad \text{Eq. (5b)}$$

$$A_1 = 0.180 \left(\frac{H_{m0}}{h} \right)^{-0.391} \quad \text{Eq. (5c)}$$

Herrera et al. (2017) carried out new tests in shallow water and introduced a new design formula for breaking waves using a combined experimental-numerical approach with SwanOne (Booij et al., 1999), neglecting the effects of low-frequency waves. The work includes 44 data with a 1V:50H foreshore slope and a breakwater with a 1V:1.5H slope angle on an underlayer and core. The dataset is not included in the present study since they performed subsequent tests, without rebuilding the armor layer and, hence, cannot be fully compared with the other datasets.

In Eldrup and Andersen (2019), hereafter referred to as EA, the hydraulic stability in shallow water was investigated with a focus on the effects of nonlinear waves and very low wave steepness. The authors revisited the original VDM stability formulae and developed a new formulation (Eqs. (6a,b)) based on the newly acquired dataset (68 data) and the datasets provided by VSK and Eldrup et al. (2019):

$$\frac{H_{m0}}{\Delta D_{n50}} = 4.5 \left(\frac{S}{\sqrt{N_w}} \right)^{0.2} 1.6^P \xi_{m-1,0}^{(0.4P-0.67)} \quad \text{plunge if } \xi_{m-1,0} \leq \xi_{m-1,0,c} \quad \text{Eq. (6a)}$$

$$\frac{H_{m0}}{\Delta D_{n50}} = 3.1 \left(\frac{S}{\sqrt{N_w}} \right)^{0.2} P^{0.17} \min[\cot\alpha, 2]^{0.23} \quad \text{surge if } \xi_{m-1,0} > \xi_{m-1,0,c} \quad \text{Eq. (6b)}$$

The critical surf similarity parameter ($\xi_{m-1,0,c}$) was redetermined by setting the equality of Eq. (6a) and Eq. (6b) and solving the SSP as

$$\xi_{m-1,0,c} = \left(\frac{0.69 P^{0.17} \min[\cot\alpha, 2]^{0.23}}{1.6^P} \right)^{\frac{1}{0.4P-0.67}}. \quad \text{They used foreshore slopes of}$$

1V:100H and 1V:30H, similar to VSK. As for Herrera et al. (2017), the data are not used in the present study since they evaluated cumulative damage.

Alternative approaches utilizing AI computing techniques, such as Artificial Neural Networks or other machine learning models (Mase et al., 1995; Lee et al., 2016; Wei et al., 2019) and genetic programming (Lee and Suh, 2020), have gained attention. In Etemad-Shahidi et al. (2020), hereafter referred to as ES, a multi-variable regression model was employed on an experimental database gathering the data of TS, VDM, VSK and Vidal et al. (2006), hereafter referred to as VML. The database comprises a total of 1199 tests, of which 72% in deep water and formed the basis of the VDM formula. Only 17% of the tests is related to the tests of VSK. The final synthesized database has 791 data points with $2 \leq S \leq 12$. The aim was to develop a compact and concise formula suitable from deep to shallow water conditions for both plunging (Eq. (7a)) and surging (Eq. (7b)) waves:

$$\frac{H_s}{\Delta D_{n50}} = 4.5 C_p N_w^{\frac{1}{10}} S^{\frac{1}{6}} \xi_{s-1,0}^{\frac{7}{12}} (1-3m) \quad \text{plunge if } \xi_{s-1,0} < 1.8 \quad \text{Eq. (7a)}$$

$$\frac{H_s}{\Delta D_{n50}} = 3.9 C_p N_w^{\frac{1}{10}} S^{\frac{1}{6}} \xi_{s-1,0}^{\frac{1}{3}} (1-3m) \quad \text{surge if } \xi_{s-1,0} \geq 1.8 \quad \text{Eq. (7b)}$$

where $C_p = \left[1 + (D_{n50,core}/D_{n50})^3 \right]^{3/5}$ is the permeability coefficient.

These formulae incorporate the effect of the foreshore slope $m=\tan\beta$, with β the approach slope angle.

To gain more insight into stone armor stability, particularly in very and extremely shallow water conditions with heavy wave breaking on the foreshore, Marino et al. (2022) and Scaravaglione et al. (2024, 2025) carried out a new physical experimental campaign collecting a new dataset, hereafter referred to as EUMER. Based on these experiments, Scaravaglione et al. (2025) proposed a modified version of the van Gent equation, hereafter referred to as the Modified van Gent, which explicitly includes wave steepness, as shown in Eq. (8):

$$\frac{H_{m0}}{\Delta D_{n50}} = 3.3\sqrt{\cot\alpha} \left(1 + \frac{D_{n50,core}}{D_{n50}}\right) s_{m-1,0}^{0.1} \left(\frac{S}{\sqrt{N_w}}\right)^{\frac{1}{5}} \quad \text{Eq. (8)}$$

additionally, the authors developed a modified version of the ES equation, hereafter referred to as the Modified ES. For plunging waves, the original ES formulation is retained but rewritten in terms of H_{m0} (Eq. (9a)), while for surging waves, a new expression (Eq. (9b)) is proposed, explicitly incorporating wave steepness and structural slope effects, with the two variables treated independently.

$$\frac{H_{m0}}{\Delta D_{n50}} = 4.5C_p N_w^{-\frac{1}{10}} S_6^{\frac{1}{2}} \xi_{s-1,0}^{-\frac{7}{12}} (1-3m) \quad \text{plunge if } \xi_{m-1,0} < 1.8 \quad \text{Eq. (9a)}$$

$$\frac{H_{m0}}{\Delta D_{n50}} = 3.55C_p N_w^{-\frac{1}{10}} \cot\alpha^{\frac{1}{3}} S_6^{\frac{1}{2}} s_{m-1,0}^{\frac{1}{20}} (1-3m) \quad \text{surge if } \xi_{m-1,0} \geq 1.8 \quad \text{Eq. (9b)}$$

The work includes 55 data with a 1V:30H foreshore slope, and 4 water levels, with 4 permeable cross-sections at 1V:2H slope angle. Test conditions also include severe wave breaking (extremely shallow conditions) with a relative depth h_r up to approximately 5.

None of the laboratory-based wave stability formulae evaluated herein can reliably describe armor stability across all water depth conditions without significant uncertainty. Indeed, engineering manuals outline some of the above-mentioned stability formulae, each tailored to specific ranges of validity and application scenarios. These manuals provide guidance on the fundamental methodologies for evaluating the stability of stone-armored slopes and offer an overview of the applications for different stability formulae, advising on when and how to employ them. However, these resources are not only outdated but also present overlapping regions where different stability formulae can be utilized, resulting in significantly divergent outcomes. Semi-empirical formulae have often been incorporated into probabilistic frameworks that consider the concurrent effects of intrinsic and epistemic uncertainty considering fit coefficient standard deviations based on the specific data tested. Nevertheless, the amalgamation of epistemic and intrinsic uncertainty within a single probabilistic framework is typically a practical choice rather than an intentional one due to the impossibility of proceeding otherwise. Therefore, the comprehensive investigation into the relative importance of epistemic versus intrinsic uncertainty remains a literature gap and an ongoing challenge that would guide studies toward improving physics research.

The present paper aims to improve the understanding and quantification of uncertainties in stone armor stability by synthesizing data from a wide range of experimental studies. The methodology involved collecting data and homogenizing parametric characteristics to create a new unified database. Eqs (1a,b)–(4a,b), (6a,b), (7a,b), (8), (9a,b) are considered in the present study, compared, and recalibrated to evaluate their predictive performance also when applied to independent datasets, including cases that fall outside their original validity ranges and highlight strengths and weaknesses across all water depth conditions. The manuscript is organized as follows: Section 2 details the synthesis and formation of the database across various wave and water depth conditions; in Section 3 the new database is used to evaluate the performance of the selected design formulations, followed by their refitting, and results are discussed in the context of quantifying uncertainty for

Table 1
Summary of the main characteristics of the stability equations and the new database.

Main characteristics of stability formulae	New database					
	Modified van Gent (2025) & Modified ES (2025)	ES (2020)	EA (2019)	MK (2011)	Modified VDM (2003) & Simple van Gent (2003)	Rewritten VDM (2021)
Datasets used for formulae calibration	EUMER	VDM, TS, VSK, VML	VSK, EA, Eldrup et al. (2019)	VDM	VDM, VSK	TS, VDM
Structure slope, $\cot\alpha$	2	1.5–6	1.5–6	1.5–6	1.5–6	1.5–6
Foreshore slope, $\cot\beta$	30	Flat, 100, 30	100, 30	Flat, 30	Flat, 100, 30	Flat, 30
Permeability	$(D_{n50,core}/D_{n50})$	$(D_{n50,core}/D_{n50})$	P estimated	P	$P, (D_{n50,core}/D_{n50})$	P
Water depth	Intermediate, shallow, very shallow, extremely shallow	Deep, shallow, very shallow	Shallow, very shallow	Deep, shallow	Deep, shallow, very shallow	Deep, shallow
Number of tests, N	55	791	68 (635)	294	207 (567)	360
Damage analysis	Homogenous	Non-homogeneous	Homogeneous	Homogeneous	Homogeneous	Non-homogeneous
General potential sources of uncertainty in the database	Wave analysis	Damage measurement, Damage analysis, Test execution	Damage measurement, Damage analysis	Damage measurement	Damage analysis	Wave generation, Damage analysis

design purposes; Section 4 reports the key findings and identifies future research lines.

2. Description of the new database

Data synthesis involved collecting information from 4 different studies and homogenizing parametric characteristics to the extent possible, considering the disparate nature of the native data. The following test conditions were considered:

- 2D physical model;
- Head-on wave attack;
- Irregular wave trains;
- Emerged rock-armored structures with permeable or impermeable core;
- No to little overtopping;
- Absence of a berm (if $B < 1.3D_{n50}$), where B represents berm width;
- Standard equant shape armor layer ($c_{pl}=1, c_{su}=1$);
- 2-2.5 D_{n50} armor layer thickness;
- Bulk-random placement of stones;
- Number of waves N_w within range 500–5000;
- Constant wave and water level conditions for each test and damage measurement starting from zero damage.

A total of 691 irregular wave tests refer to the above conditions and were organized for subsequent analyses. The datasets selected and utilized include:

- TS dataset – 135 data (Thompson and Shuttler, 1975)

Table 2
Damage range considered in the analysis.

Armor slope	$S_{initial}$	$S_{intermediate}$	$S_{failure}=S_{max}$	$1.5S_{max}$
1V:1.5H	2	3 to 5	8	12
1V:2H	2	4 to 6	8	12
1V:3H	2	6 to 9	12	18
1V:4H	3	8 to 12	17	25.5
1V:6H	3	8 to 12	17	25.5

Table 3
Main model characteristics of the datasets.

Parameter	TS	VDM	VSK	EUMER	Total
$cota$	2–6	1.5–6	2, 4	2	1.5–6
$cot\beta$	Flat	Flat, 30	100, 30	30	Flat, 100, 30
Δ	1.70	0.92–2.05	1.65–1.75	1.574	0.92–2.05
D_{85}/D_{15}	2.24	1.25–2.25	1.4–2	1.20–1.28	1.20–2.25
$D_{n50,core}/D_{n50}$	0	0.0–1	0.0–0.45	0.22–0.72	0–1
S	≤ 17	≤ 24	≤ 26	≤ 20	≤ 26
P	0.1	0.1–0.6	0.1–0.5	0.4–0.5	0.1–0.6
LT	≤ 2	≤ 2	2.1	1.35–1.46	1.35–2.1
BLC (%)	Not available	50–60	Not available	35–45	35–60
Number of data	135	294	207	55	691

Table 4
Main waves characteristics of the datasets.

Parameter	TS	VDM	VSK	EUMER	Total
N_w	1000, 3000	1000, 3000	492–5172	595–3826	492–5172
Spectral shape ^a	PM	PM	JONSWAP, TMA, DOUBLE	JONSWAP	PM, JONSWAP, TMA, DOUBLE
$S_{m,deep}$	0.007–0.05	0.004–0.06	0.02–0.07	0.03–0.06	0.004–0.06
$S_{m-1,0,deep}$	0.006–0.045	0.003–0.055	0.017–0.052	0.020–0.050	0.003–0.055
$H_{m0,deep}/h$	0.04–0.21	0.06–0.72	0.18–2.89	0.41–4.94	0.04–4.94
$H_{m0,toe}/H_{m0,deep}$	1	1	0.22–1.06	0.20–1.03	0.20–1.06
$H_{2\%,toe}/H_{s,toe}$	1.40	1.40	1.16–1.43	1.20–1.43	1.16–1.43
$H_{m0,toe}/H_{s,toe}$	1	1	0.99–1.48	0.89–1.11	0.89–1.48
$T_{m-1,0,toe}/T_{m-1,0,deep}$	1	1	1.01–4.92	1–3.40	1–4.92
$T_{m,deep}/T_{m-1,0,deep}$	0.93–0.96	0.75–1.02	0.69–0.93	0.86–0.93	0.69–1.02

^a PM=Pierson-Moskowitz; TMA=Texel-Marsen-Arsloe; DOUBLE=Double peaked.

- VDM dataset – 294 data (van der Meer, 1988)
- VSK dataset – 207 data (van Gent et al., 2003)
- EUMER dataset – 55 data (Scaravaglione et al., 2025)

An in-depth analysis of the datasets was conducted, to standardize parameters as much as possible and facilitate meaningful comparisons. Table 1 summarizes the main characteristics of Eqs. (1a,b)–(4a,b), (6a,b), (7a,b), (8), (9a,b) and the new database described herein. The term “homogeneous” in the context of damage analysis specifically refers to the general technique employed to measure the damage. However, it is important to clarify that the same technique could also result in variability and uncertainty due to differences in aspects such as the type of profiler (e.g., mechanical or laser), the number and spacing of transects analyzed, the post-processing methods applied, and other procedural details. These factors can significantly influence the outcomes, thus introducing potential inconsistencies in the overall process. Over recent decades, the broad diversity of laboratory modeling technologies further contributes to such an unknown uncertainty. Sources of uncertainty include, but are not limited to, differences in wave generation and measurement techniques, damage quantification methodologies, experimental setups, and data analysis protocols. Quantifying the exact influence of these factors on the overall uncertainty remains extremely challenging and would require a comprehensive specific review of each individual dataset. To offer a qualitative overview of the main sources of uncertainty affecting the derivation of stability equations, Table 1 identifies the likely principal contributing factors inherent in the new database. This highlights the limitations associated with the available data and underscores the need for greater consistency in experimental practice. While the development of standardized procedures for experimental execution and data processing is a clear objective for future research, a few broadly accepted best practices are proposed as preliminary steps toward improved harmonization. These include (i) performing calibration wave tests without the structure in place, (ii) using active wave reflection compensation systems, (iii) adopting second-order wave generation techniques, (iv) acquiring at least of nine cross-sectional profile measurements, and (v) promoting consistency in wave characterization and damage analysis and evaluation methods. These recommendations are intended to support better comparability

across studies, without introducing rigid protocols that exceed the intended scope of the present study.

2.1. Synthesized database

The new database contains experimental measurements from experiments conducted in deep, intermediate, shallow, very shallow, and extremely shallow water conditions, both with and without wave breaking on the foreshore, covering a wide variety of generated wave spectra, wide armor stone gradations, providing comprehensive coverage of different armor configurations.

For design purposes, van der Meer (1988) introduced a damage classification for standard rubble mound breakwaters, categorizing damage into three levels i.e., initial, intermediate and failure, based on the armor slope of the structure. In the present study, only damage $1 \leq S \leq 1.5S_{max}$ was selected for the analyses (Table 2) to reduce the uncertainty associated with extreme damage values since such data could be affected by measurement reliability.

Tables 3 and 4 present the model characteristics, both wave and damage measurements considered in the present study, where D_{85}/D_{15} is the grading uniformity coefficient, LT and BLC are the length-to-thickness ratio and the blockiness coefficient, respectively. Although some characteristics of each study are unknown, such as certain structural and wave information, it is assumed in the analysis that the

experimental data are generally comparable. Indeed, missing information regarding the structure may not significantly impact the comparison. This assumption is based on the understanding that most researchers adhere to basic standards, and variations from laboratory to laboratory for construction of cross-sections are typically small. In our analysis, the assumptions were made to standardize the comparison to the extent possible considering the varying nature of the original data. To achieve comparable wave parameters across datasets with missing wave parameters (such as for example TS and VDM), waves are assumed to be Rayleigh distributed at the wave generator in deep and intermediate water, namely $H_{m0}=H_s$, $H_{2\%}=1.4H_s$, and $T_{m-1,0}=1.1T_m$. The mean period T_m is often used to estimate storm duration by calculating the number of waves impacting the structure. Since armor stability is not significantly influenced by minor variations in the number of waves, and because calculating the mean period (or the number of waves) in shallow water introduces considerable uncertainty, it is recommended to use the mean period in deeper water to estimate storm duration by wave count.

2.2. Wave variation with respect to relative depth

The present database was analyzed by grouping data according to the relative depth h_r in deep, intermediate, shallow, very shallow, and extremely shallow conditions. For very shallow and extremely shallow

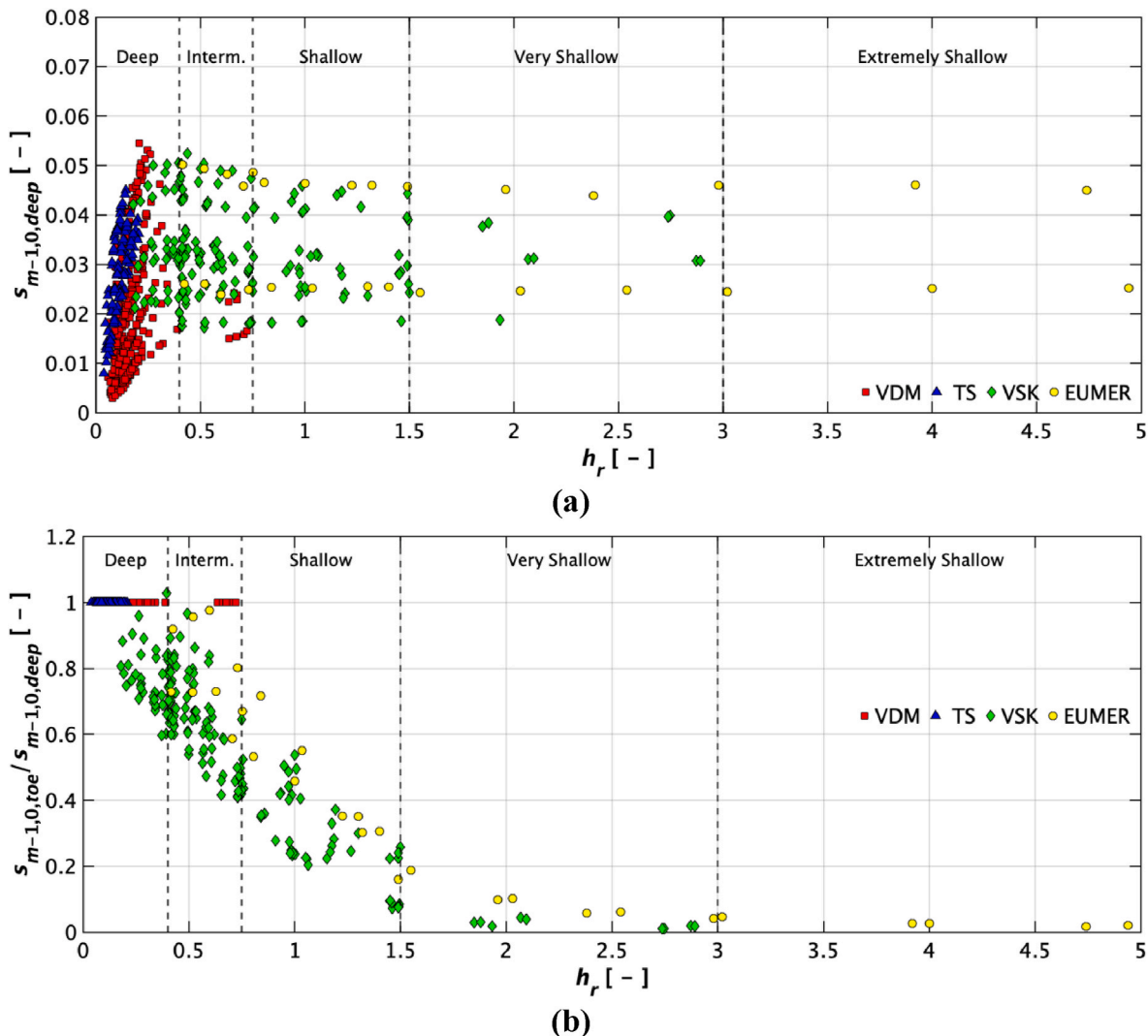


Fig. 2. Wave steepness parameters as a function of the relative depth: (a) $s_{m-1,0,deep}$; (b) $s_{m-1,0,toe}/s_{m-1,0,deep}$

water, infragravity (IG) waves come into play or even dominate the spectral energy transformation processes. IG waves are caused by nonlinear interactions that generate subharmonic wave components with wave frequencies below the wind-generated sea and swell waves (see e.g., de Ridder et al., 2024). Thus, h_r is an important parameter for describing wave behavior over a foreshore and may play a significant role in the stability of stone slopes in shallow water. However, if the influence of water depth is adequately incorporated into the wave parameters, it is argued that explicitly including local water depth in the stability expression may not be necessary. Goda (2010) presents a practical approach for describing the variation in wave height from deep water to very shallow water, identifying different zones for wave steepness greater than 1%: (i) non-breaking with no significant shoaling ($h_r < 0.17-0.25$); (ii) shoaling and slightly breaking ($h_r < 0.2-0.5$); (iii) depth-limited wave conditions with breaking ($h_r < 0.5-0.67$), where the start of breaking is due to the wave steepness; (iv) severely breaking,

where IG waves become significant ($h_r < 1$); and (v) broken waves dominated by IG waves ($h_r > 2$). In the present database, which comprises a total of 691 data, 69% of the database (475 data) correspond to deep water, 16% (112 data) to intermediate water, 11% (76 data) to shallow water, 3.1% (22 data) to very shallow water, and only 0.9% (6 data) to extremely shallow water. Nonbreaking conditions represent 85% of experimental conditions likely because nonbreaking waves are less complicated from a modeling perspective. However, this dominance should be addressed in data fitting by weighting data in order to avoid favoring non-breaking wave cases.

Fig. 2 illustrates the range covered by the database of the offshore spectral wave steepness $s_{m-1,0,deep} = H_{m0,deep}/L_{m-1,0,deep}$ (Fig. 2a) and the relative wave steepness $s_{m-1,0,toe}/s_{m-1,0,deep}$ (Fig. 2b) as a function of the relative depth (h_r). Fig. 2a shows that the database encompasses a wide range of wave steepness and the majority of design scenarios. The VSK and EUMER datasets primarily cover shallow to very and extremely

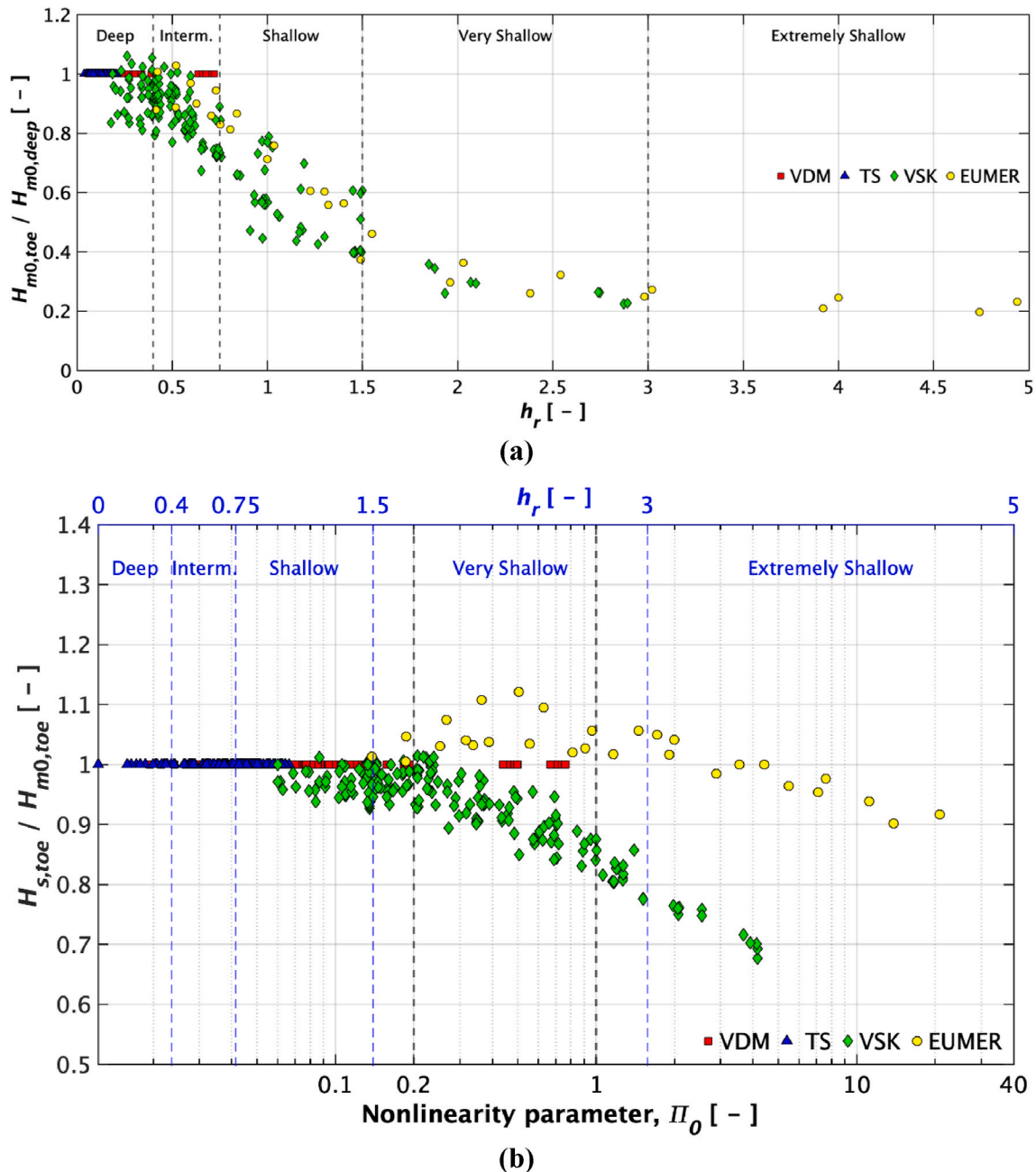


Fig. 3. Wave height ratio characteristics: a) $H_{m0,toe}/H_{m0,deep}$ as a function of the relative depth; b) $H_{s,toe}/H_{m0,toe}$ as a function of the nonlinearity parameter.

shallow foreshore conditions but exclude low steepness waves, covered, instead, by VDM dataset down to $s_{m-1,0,deep}=0.01$, specifically in deep water.

Fig. 2b shows the spectral wave steepness at the toe of the structure normalized by the corresponding offshore value as a function of the relative depth. Both parameters were calculated using H_{m0} and $L_{m-1,0}$, where $L_{m-1,0}$ was calculated from the deep water wavelength formula. On shallow foreshores, wave height significantly decreases while wave period increases, resulting in a spectral steepness much lower than $s_{m-1,0,deep}$. In very and extremely shallow water, changes in the spectral shape become pronounced, leading to very low wave steepness values at the toe. This reduction reflects a clear shallow water effect, where the wave steepness becomes low and deviates from formulae calibrated for deeper water conditions. This phenomenon is driven by bound long waves that become free long waves, dissipation of the energy in sea and swell waves, and triad nonlinear wave interactions, where energy is redistributed to both higher and lower harmonics. Wave breaking dissipates most of the swell and sea energy, allowing lower harmonic components to dominate as waves propagate further into the surf zone. Although some wave components reform and break again, the overall energy shift toward lower frequencies results in a spectral period much higher than short waves. The total wave steepness, dominated by low-frequency energy, becomes less representative of the wave field in shallow water, emphasizing the need for localized parameterization to capture the dynamics of short waves accurately.

Fig. 3 presents the relative wave heights ($H_{m0,toe}/H_{m0,deep}$ and $H_{s,toe}/H_{m0,toe}$) as a function of h_r (Fig. 3a) and the nonlinearity parameter Π_0 (Fig. 3b). Fig. 3a reveals an exponential decrease as the relative water depth increases. This provides insight into the amount of wave breaking on the foreshore. Depth-limited wave breaking results in energy dissipation along the foreshore and the trend is fairly consistent and well-defined across the database. Observing the graph from left to right, it is evident that, in deep water, wave breaking does not occur, although some cases exhibit slight shoaling on the foreshore before reaching the toe of the structure, as indicated by ratios $H_{m0,toe}/H_{m0,deep} > 1$ in certain VSK and EUMER data. While most tests follow a consistent relationship, deviations are observed for tests with 1V:30H and 1V:100H slopes up to very shallow water. In the 1V:30H series, wave heights are slightly higher compared to the 1V:100H series in shallow water due to more pronounced shoaling and a narrower surf zone. This results in more wave energy at the shallow end of the steeper foreshore compared to the gentler slope. But in general, all foreshore slopes exhibit a significant reduction in wave energy of up to 80%. In deeper water, wave steepness influences the dissipation of wave energy. Low steepness waves retain more energy compared to high wave steepness waves, as wave breaking under deep water conditions is primarily governed by wave steepness. The graph clearly shows that wave breaking and depth-limited

conditions occur for $h_r > 0.4$.

Fig. 3b shows the ratio $H_{s,toe}/H_{m0,toe}$ plotted against the nonlinearity parameter for all tests, with the relative depth also displayed on the upper x-axis. This figure highlights that the differences between $H_{s,toe}$ and $H_{m0,toe}$ can be significant, especially for shoaled low steepness waves. This underscores the importance of considering the distinction between the two wave heights in shallow water conditions. Goda (2010)

defined the nonlinearity parameter as $\Pi_0 = \frac{H_{m0,deep}}{L_{m,deep}} \coth\left(\frac{2\pi h}{L_{m,deep}}\right)^3$, where $L_{m,deep}$ is the local wavelength calculated with T_m . For $\Pi_0 \leq 0.2$, data indicate that the ratio $H_{s,toe}/H_{m0,toe}$ is approximately 1. However, a clear difference emerges in the range $0.2 < \Pi_0 < 1$, where the ratio increases for EUMER data, but suddenly decreases for VSK data, reflecting the expected mean behavior for low steepness waves described by Goda (2010). For $\Pi_0 \geq 1$, two distinct trends are observed, namely the ratio decreases to around 0.9 for EUMER data and to around 0.7 for VSK data. In relatively shallow water, wave nonlinearity increases with wave height. As waves approach the shore, they undergo nonlinear shoaling, resulting in wave profiles with high and sharp crests and low and flat troughs. This nonlinearity is most pronounced near the outer edge of the surf zone. Within the surf zone, as waves begin to break, nonlinearities diminish progressively, depending on wave steepness. Low steepness waves, in particular, experience significant nonlinear shoaling before breaking, while high steepness waves tend to break earlier.

Fig. 4 and Fig. 5 show the ratio $H_{2\%,toe}/H_{s,toe}$ and the relative wave period ($T_{m-1,0,toe}/T_{m-1,0,deep}$) plotted against h_r . In addition to the reduction in wave height, it is well known that wave height distribution also changes in shallow water. Under deep water conditions, where wave breaking is absent, wave heights can be assumed to be Rayleigh distributed for linear narrow-banded spectra, with this ratio equal to 1.40 (solid black line). As waves propagate and shoal, the nonlinear shoaling process enhances individual wave heights, causing deviations from the Rayleigh distribution. Once waves enter the surf zone, the wave breaking process significantly alters the wave height distribution and the ratio can decrease from 1.40 to approximately 1.20 for depth-limited conditions ($h_r < 0.75$). Beyond this range, the ratio begins to increase again and tends to stabilize in extremely shallow water ($h_r > 3$), approaching the original value of 1.4, consistent with Goda (2010, 2012), which indicates that the wave height distribution returns to Rayleigh as waves approach the shoreline. In extremely shallow water, however, $H_{2\%}$ is much larger than the one predicted by a Rayleigh distributed wave field (de Ridder et al., 2024; Scaravaglione et al., 2025). This behavior is relevant as $H_{2\%}$ is a characteristic parameter to describe the highest waves that contribute to armor stability. On the other hand, the trend observed here could not be described by Battjes and Groenendijk (2000), as their dataset did not include data for

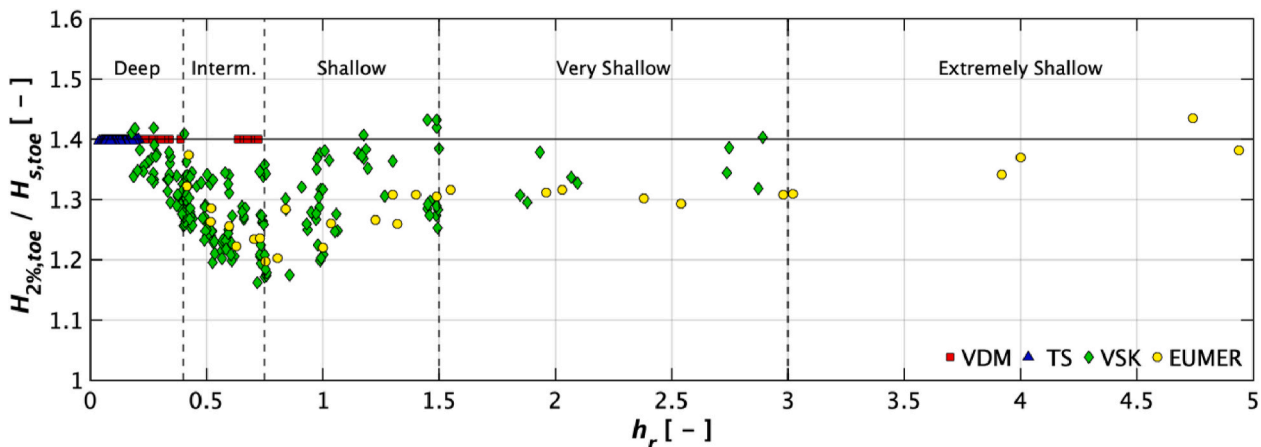


Fig. 4. $H_{2\%,toe}/H_{s,toe}$ as a function of the relative depth.

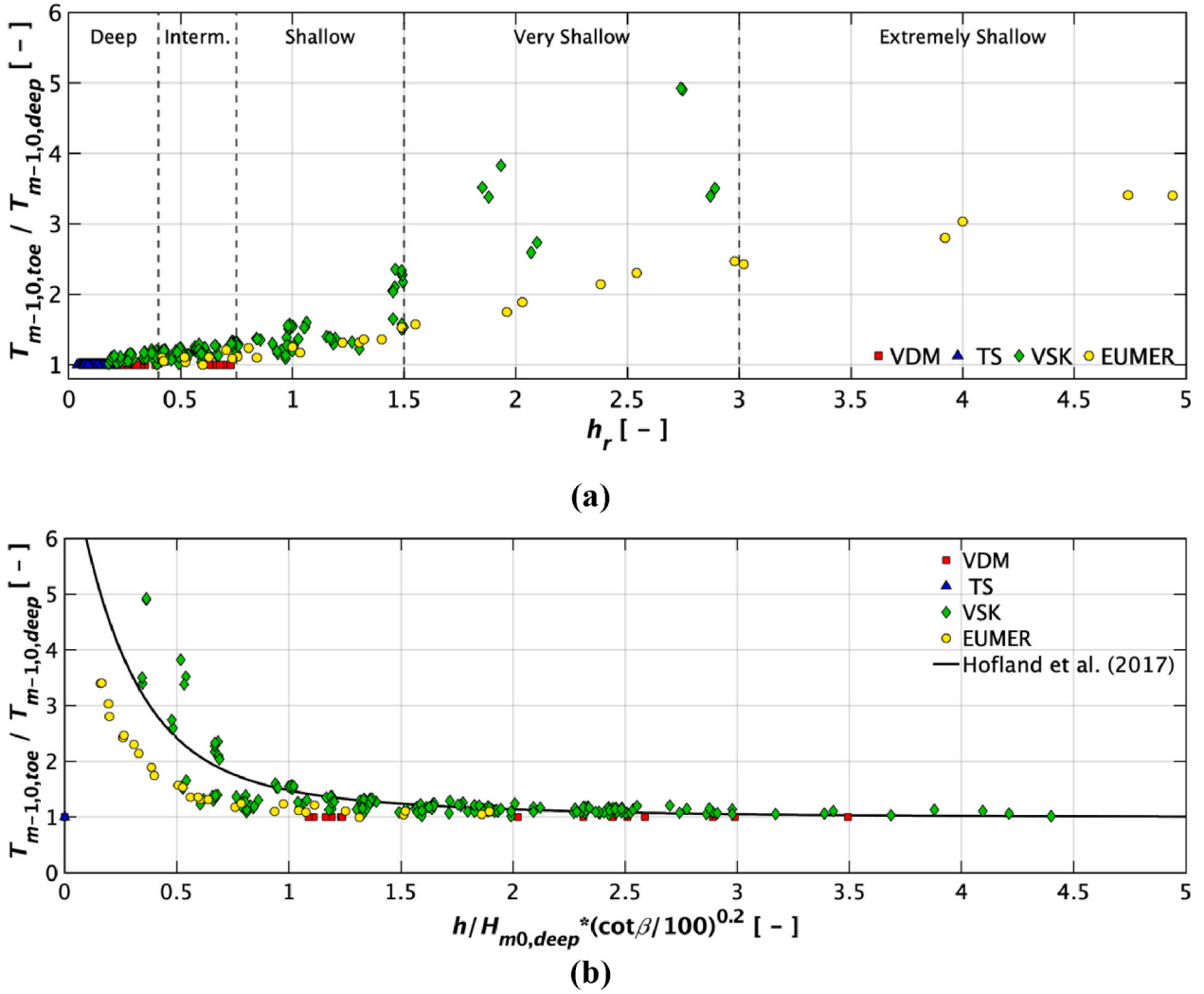


Fig. 5. a) Relative wave period as a function of the relative depth. b) Comparison with Hofland et al. (2017).

$h_r > 0.75$. Consequently, extrapolation of their method to high relative depths could lead to significant underprediction of $H_{2\%,toe}$.

Fig. 5a demonstrate how, in wave flumes, IG waves significantly influence wave parameters, especially $T_{m-1,0,toe}$. As waves propagate along the flume, the spectral wave period at the toe increases, reaching nearly five times the deep water period under very/extremely shallow conditions. This increase is caused by wave transformation along the foreshore, where most of the energy near the spectral peak is dissipated due to wave breaking, while IG energy is amplified. This behavior becomes more pronounced as h_r increases, particularly in very and extremely shallow conditions.

Fig. 5b compares the experimental data against the predictions by Hofland et al. (2017), expressed as $\frac{T_{m-1,0,toe}}{T_{m-1,0,deep}} = 1 + 6 \exp(-4\tilde{h}) + \exp(-\tilde{h})$, where $\tilde{h} = \frac{h}{H_{m0,deep}} \left(\frac{\cot\beta}{100}\right)^{0.2}$ is the dimensionless depth. The comparison reveals that, as expected, the formulation aligns well with data for the mildest foreshores (e.g., 1V:100H) but overestimates the relative wave period for steeper foreshore slopes (e.g., 1V:30H). This discrepancy arises because the dataset used by Hofland et al. (2017) was based on tests conducted with mild foreshore slopes and wave overtopping conditions. Indeed, most of the data used by Hofland et al. (2017) correspond to very shallow water ($h_r > 3$) with foreshore slopes of 1V:35H, 1V:250H and 1V:300H. Only limited data were available for somewhat less severe wave breaking ($h_r < 1.5$) with gentler foreshore slopes of

1V:100H and 1V:250H (van Gent, 1999). Gentle slopes lead to a greater increase in wave period compared to steeper slopes, as demonstrated by the comparison of VSK data and EUMER data. Specifically, for the VSK data, a foreshore slope of 1V:100H gives ratios of $T_{m-1,0,toe}/T_{m-1,0,deep}$ up to 5, where it remained limited to about 3–4 for the steeper foreshore slope of 1V:30H. It can be concluded that for $h_r > 0.75$, $T_{m-1,0,toe}$ may increase up to about 50% with respect to the deep water value.

The relative ranges for each parameter are summarized in Table 4.

3. Results

3.1. Comparison between original stability formulae

This section presents a comparison of the most widely used stability formulae described in Section 1, evaluated using main error metrics as a measure of the total uncertainty which includes both intrinsic and epistemic uncertainty components. The strengths and weaknesses of various approaches across different water-depth conditions are discussed, highlighting the main causes of deviations. Data were classified based on the shallowness criterion, defined by h_r , with intermediate and extremely shallow water grouped together with shallow and very shallow water, respectively. As a result, stability equations, including the Modified van der Meer (Eq. (2a,b), van Gent et al., 2003), Simple van Gent (Eq. (3), van Gent et al., 2003), Melby and Kobayashi (2011) Eq. (4a,b), Eldrup and Andersen (2019) Eq. (6a,b), Etemad-Shahidi et al.

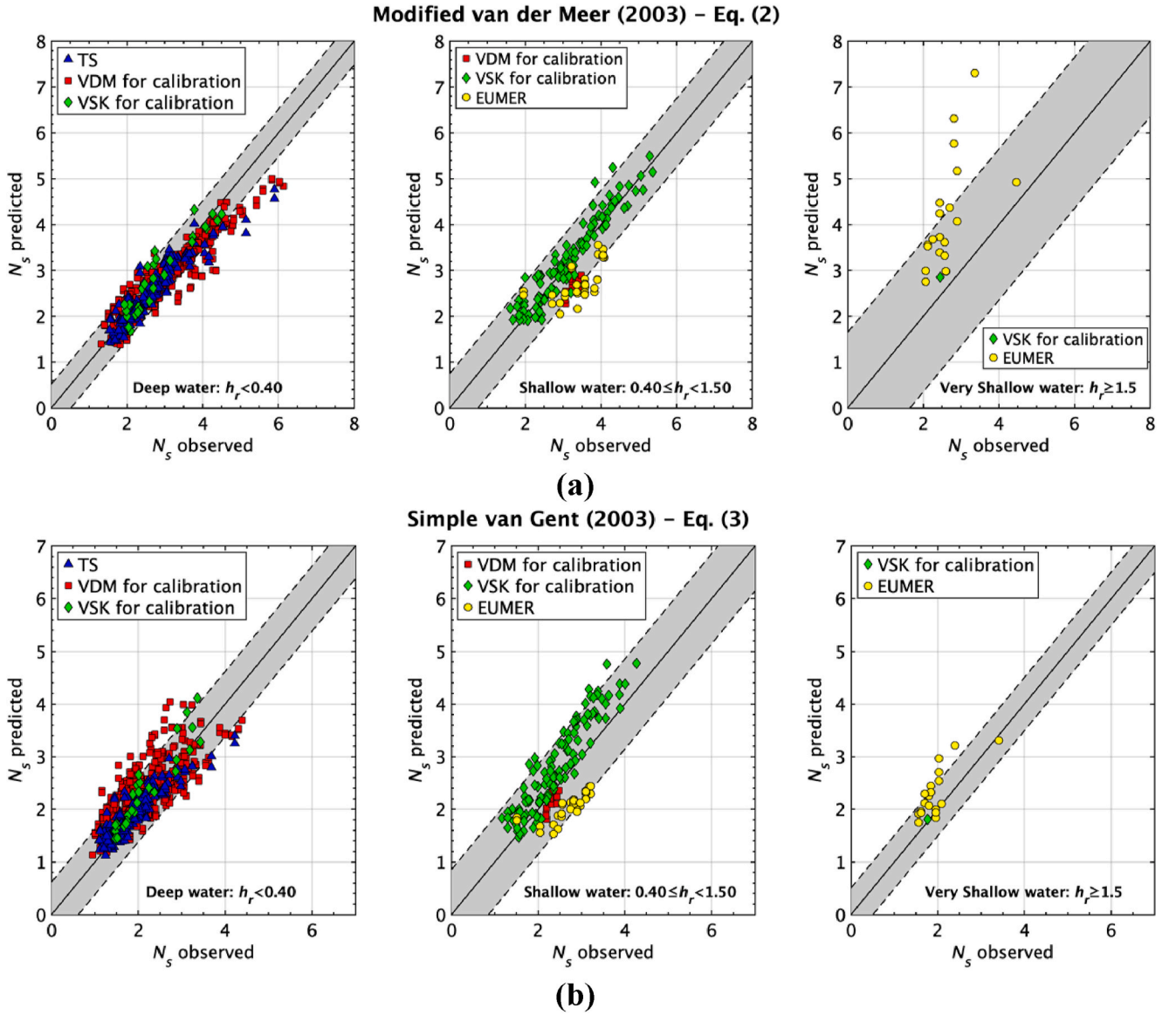


Fig. 6. Comparison between observed and predicted stability numbers by: a) Modified van der Meer (2003) (van Gent et al., 2003); b) Simple van Gent (2003) (van Gent et al., 2003); c) Melby and Kobayashi (2011); d) Eldrup and Andersen (2019); e) Etamad-Shahidi et al. (2020); f) Rewritten van der Meer (2021) (van der Meer, 2021); g) Modified van Gent (2025) (Scaravaglione et al., 2025); h) Modified ES (2025) (Scaravaglione et al., 2025).

(2020) Eq. (7a,b), Rewritten van der Meer (Eq. (1a,b), van der Meer, 2021), Modified van Gent (Eq. (8), Scaravaglione et al., 2025) and Modified ES (Eq. (9a,b), Scaravaglione et al., 2025) are plotted in Fig. 6. The datasets used to calibrate/verify each stability equation are indicated in the legend for clarity, emphasizing the differences in data sources and calibration techniques. This approach facilitates a better understanding of the applicability and limitations of each stability equation across varying water depths and experimental setups.

Fig. 6 illustrates the measured vs. predicted stability number (N_s) for each equation, presented separately for deep (left), shallow (center), and very shallow (right) water conditions. For each graph, the 90% confidence bands are reported providing a visual representation of the uncertainty range. The accuracy of the predictions was quantified using standard error metrics, including the root mean square error ($RMSE$) and the coefficient of determination (R^2), as defined in Eqs. (10a,b). Additionally, the relative bias (μ), standard deviation (Std), and coefficient of variation (CoV) were calculated (Eqs. (10c,d,e)). Based on the error ($E_i = N_{s,obs} - N_{s,pred}$), these metrics were defined as follows:

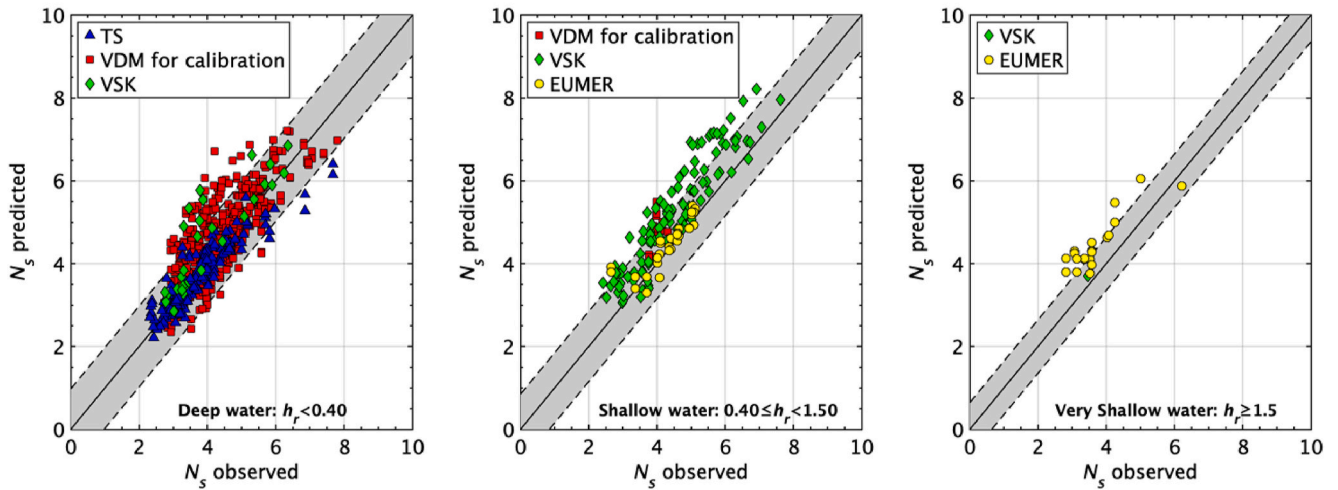
$$RMSE = \sqrt{\frac{1}{M} \sum_{i=1}^M (E_i)^2} \quad \text{Eq. (10a)}$$

$$R^2 = 1 - \frac{\sum_{i=1}^M (E_i)^2}{\sum_{i=1}^M (N_{s,obs} - \bar{N}_{s,obs})^2} \quad \text{Eq. (10b)}$$

$$Relative\ bias = \mu = \frac{\frac{1}{M} \sum_{i=1}^M (E_i)}{\bar{N}_{s,obs}} \cdot 100 \quad \text{Eq. (10c)}$$

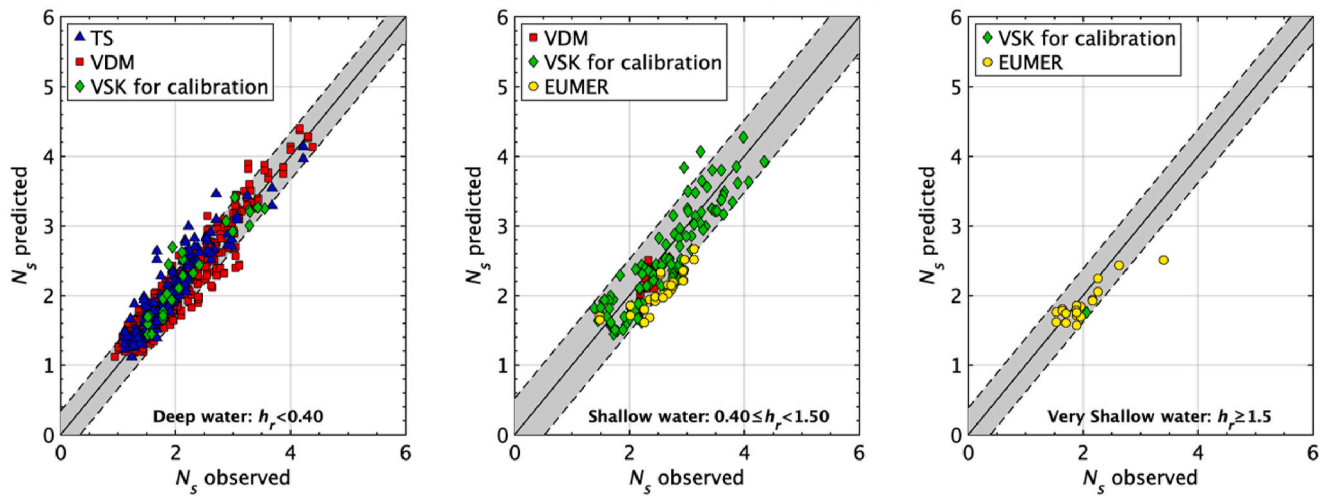
$$Std = \sqrt{\frac{1}{M-1} \sum_{i=1}^M |E_i - \bar{E}_i|^2} \quad \text{Eq. (10d)}$$

Melby and Kobayashi (2011) – Eq. (4)



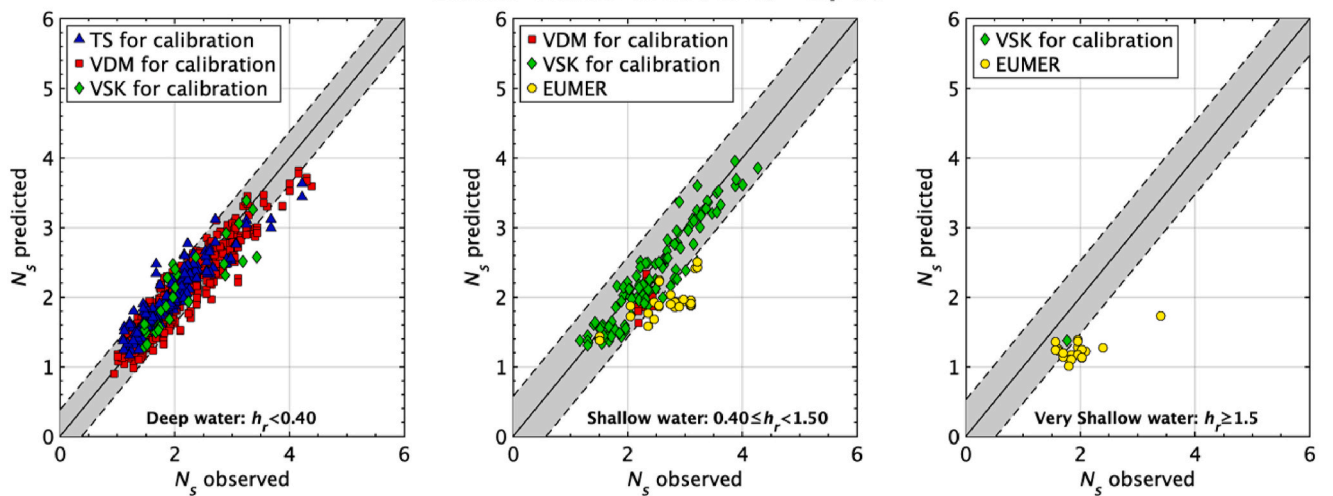
(c)

Eldrup and Andersen (2019) – Eq. (6)



(d)

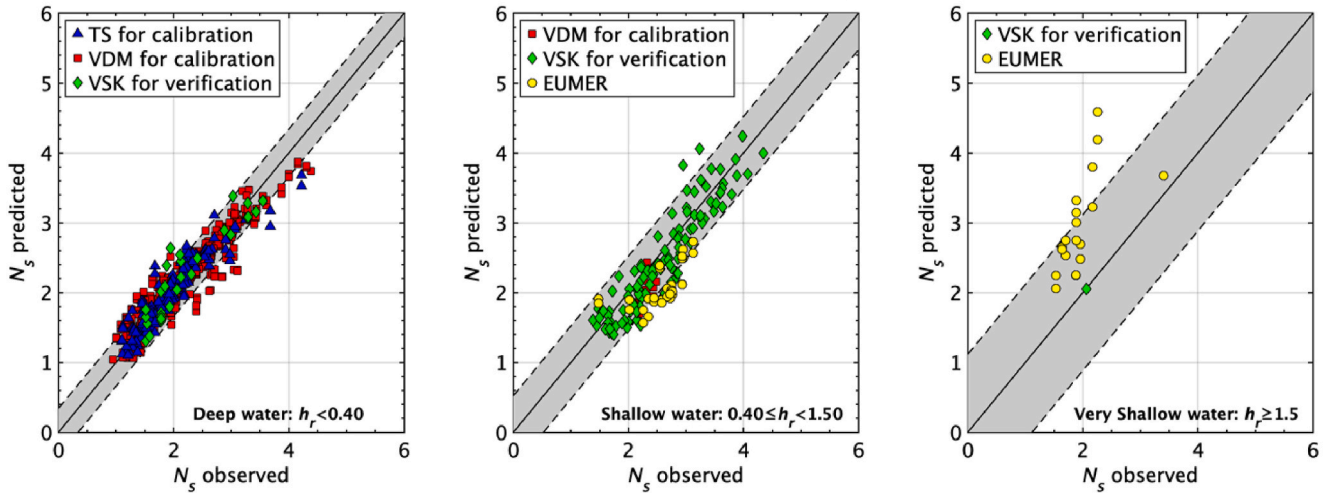
Etemad-Shadidi et al. (2020) – Eq. (7)



(e)

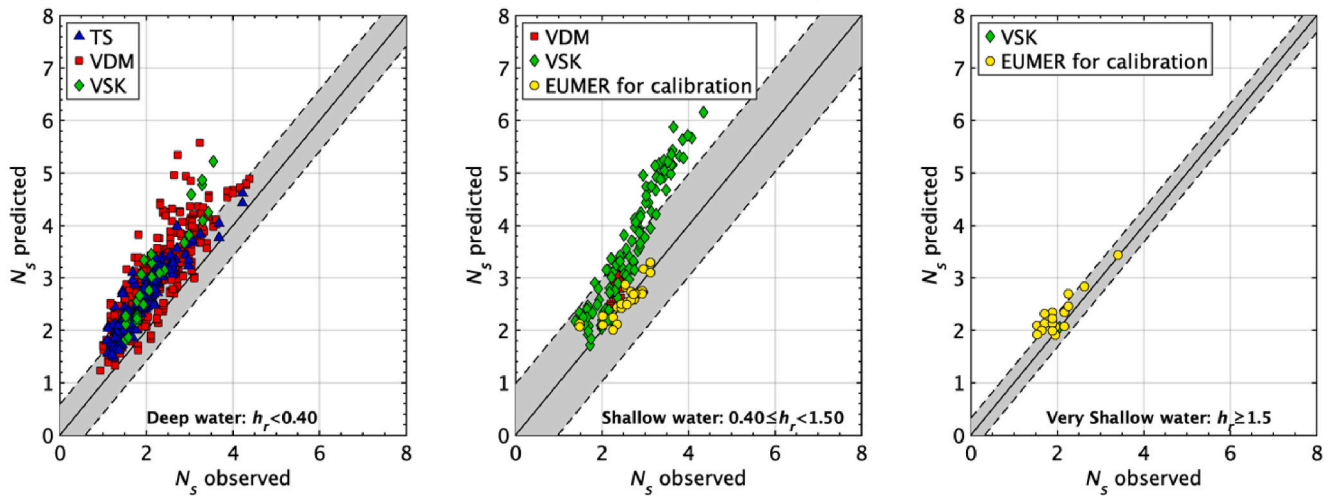
Fig. 6. (continued).

Rewritten van der Meer (2021) – Eq. (1)



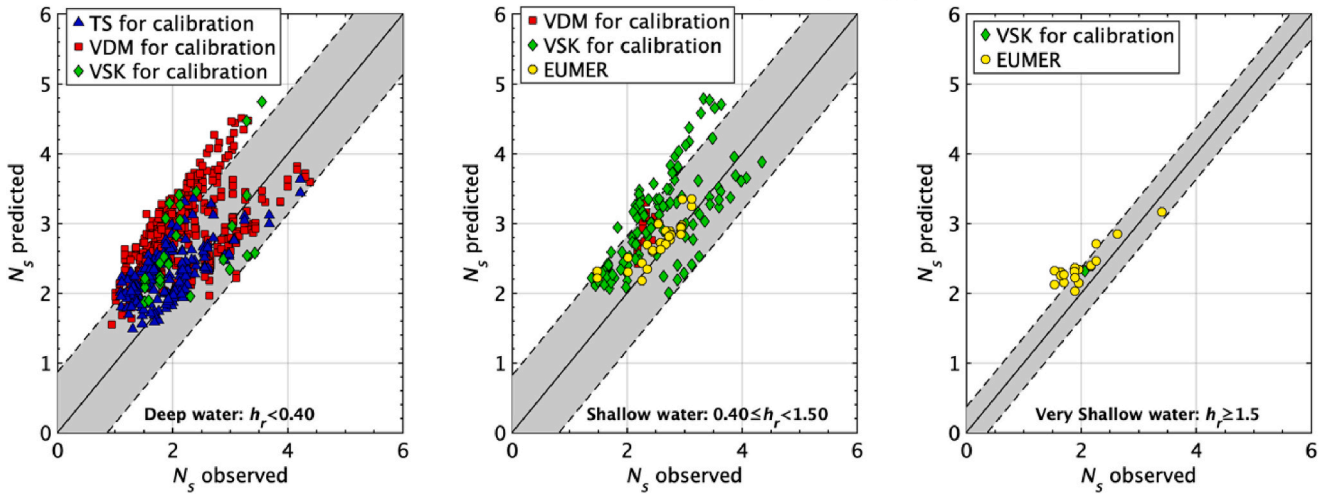
(f)

Modified van Gent (2025) – Eq. (8)



(g)

Modified Etemad-Shadidi et al. (2025) – Eq. (9)



(h)

Fig. 6. (continued).

Table 5
Error metrics for stability formulae across varying shallowness conditions.

Stability Formulae	All			Deep			Shallow			Very Shallow		
	RMSE	R ²	PSE	RMSE	R ²	PSE	RMSE	R ²	PSE	RMSE	R ²	PSE
	[-]	[-]	[-]	[-]	[-]	[-]	[-]	[-]	[-]	[-]	[-]	[-]
Modified VDM (2003) – p = 6	0.46	0.84	0.22	0.36	0.88	0.13	0.47	0.90	0.24	1.77	<0	5.63
Simple van Gent (2003) – p = 4	0.42	0.77	0.18	0.39	0.72	0.16	0.54	0.79	0.30	0.44	0.87	0.29
MK (2011) – p = 5	0.67	0.77	0.45	0.63	0.73	0.40	0.81	0.82	0.70	0.84	0.83	1.14
EA (2019) – p = 4	0.25	0.92	0.06	0.22	0.92	0.05	0.36	0.90	0.14	0.26	0.94	0.10
ES (2020) – p = 6	0.30	0.88	0.09	0.23	0.90	0.06	0.43	0.86	0.20	0.76	0.62	1.03
Rewritten VDM (2021) – p = 4	0.31	0.88	0.10	0.21	0.92	0.04	0.38	0.88	0.15	1.23	<0	2.44
Modified van Gent (2025) – p = 5	0.81	0.15	0.67	0.79	<0	0.64	0.93	0.31	0.92	0.32	0.91	0.17
Modified ES (2025) – p = 7	0.76	0.26	0.58	0.78	<0	0.63	0.67	0.64	0.48	0.26	0.84	0.33

*Colored legend for performance:
green = high R² (0.8≤R²<1), yellow = mid R² (0.6≤R²<0.8), orange = low R² (R²<0.6).
green = low RMSE (RMSE<0.35), yellow = mid RMSE (0.35≤RMSE≤0.65), orange = high RMSE (RMSE>0.6).
green = low PSE (PSE<0.3), yellow = mid PSE (0.3≤PSE<0.6), orange = high PSE (PSE≥0.6).

Stability Formulae	All		Deep		Shallow		Very Shallow	
	μ	Std	μ	Std	μ	Std	μ	Std
	[%]	[-]	[%]	[-]	[%]	[-]	[%]	[-]
Modified VDM (2003)	4.3	0.45	5.9	0.31	3.7	0.45	-56.1	1.00
Simple van Gent (2003)	-6.1	0.40	-5.7	0.38	-5.9	0.52	-16.8	0.31
MK (2011)	-7.2	0.60	-4.9	0.59	-14.2	0.52	-20.2	0.39
EA (2019)	-0.7	0.25	-3.0	0.21	6.8	0.32	6.6	0.23
ES (2020)	4.2	0.29	1.6	0.23	10.6	0.35	35.7	0.32
Rewritten VDM (2021)	0.2	0.31	-0.6	0.21	8.2	0.32	-51.7	0.68
Modified van Gent (2025)	-32.7	0.41	-34.3	0.36	-27.9	0.59	-12.9	0.19
Modified ES (2025)	-25.8	0.52	-28.1	0.53	-17.6	0.50	-18.	0.22

*Colored legend for performance:
green = low μ (|μ|<5), yellow = mid μ (5≤|μ|<10), orange = high μ (|μ|≥10).
green = low Std (Std <0.3), yellow = mid Std (0.3≤Std<0.5), orange = high Std (Std≥0.5).

$$CoV = \frac{Std(E_i)}{\sqrt{\frac{1}{M} \sum_{i=1}^M (|E_i|)}} \cdot 100 \tag{Eq. 10e}$$

where N_{sobs} and N_{spred} denote the observed and predicted stability numbers, respectively, M is the total number of observations, and \bar{N}_{sobs} is the mean of the observed stability numbers.

It is also important to highlight that the stability equations differ in their structural complexity, particularly in terms of the number of explanatory variables. While models with more parameters may offer greater flexibility and potentially improved fit to specific datasets, they also introduce additional sources of uncertainty, especially when applied to limited or non-homogeneous data (Mares-Nasarre et al., 2021). To account for this, the Predicted Squared Error (PSE) was computed following the formulation proposed by Medina et al. (2003), as given in Eq. (11):

$$PSE = MSE \left[1 + \frac{2p}{(M-p)} \right] \tag{Eq. 11}$$

where p is the number of explanatory variables in the model and MSE is the mean squared error of the residuals. Lower PSE values indicate greater expected generalizability and, consequently, more robust model performance when applied beyond the calibration dataset.

A large amount of scatter was observed in the existing formulations, which were mostly derived for conditions with little to no wave breaking on the foreshore. In comparison, the current database includes conditions with severe wave breaking and wide surf zones, contributing to the observed variability. Table 5 and Fig. 7 present the error measures (RMSE, R², PSE, μ, Std) for each stability formula, computed across all conditions as well as specifically for deep, shallow, and very shallow water conditions. Based on the criteria of the lowest RMSE, PSE, μ, and Std, and the largest R², the results indicate that most formulations perform well in deep water, but weaknesses are evident in shallow and very shallow water. To enhance visual clarity, a color gradient is applied in Table 5: green indicates high, yellow intermediate, and orange low predictive performance. It is important to emphasize that the primary aim of this study is not to establish a general rank of the stability

formulae, but rather to offer a comprehensive evaluation based on a broad set of error indicators.

3.2. Discussion

This section examines the main factors likely contributing to the observed differences in stability equations, as outlined in Section 3.1. The analysis begins with an evaluation of systematic bias and mean trends, followed by an assessment of scatter and uncertainty based on the error metrics provided in Table 5.

Notable deviations in mean trends were observed exclusively for structure slopes with $cot\alpha=6$ (27 data for VDM and 24 data for TS), in agreement with the findings of Jumelet et al. (2023). Consequently, these data should be excluded from future analyses, as they exhibit distinct physics in the stability process. Conversely, a high bias was evident in nearly all stability formulae. This can be attributed to their calibration using specific datasets rather than the comprehensive database employed in this study, limiting their applicability to narrow ranges of conditions. It is important to emphasize that the number of tests significantly influences the fitting process. Larger datasets may dominate the analysis, resulting in equations that appear to provide a better fit, even if their overall performance is suboptimal. For instance, the VDM dataset, representing approximately 43% of the total database, exerts considerable influence due to its size. However, it predominantly reflects deep water conditions and tall structures, relying on older wave and sounding technologies compared to more recent studies. These factors introduce offsetting biases that can be challenging to disentangle and correct. Moreover, not all equations and datasets are directly comparable. Stability equations should be tested only within their field of application, and datasets are often not entirely homogenous. For instance, an example of unknown uncertainty arises from variations in damage evaluation conducted using different profiling instruments across VDM, VSK and EUMER datasets.

Looking specifically at the equations, the Rewritten VDM equations using H_{m0} perform well in deep water conditions but exhibit progressively higher bias and uncertainty in shallow and very shallow conditions. This is primarily because the original equations were fitted only using VDM and TS datasets, mostly with nonbreaking waves in relatively

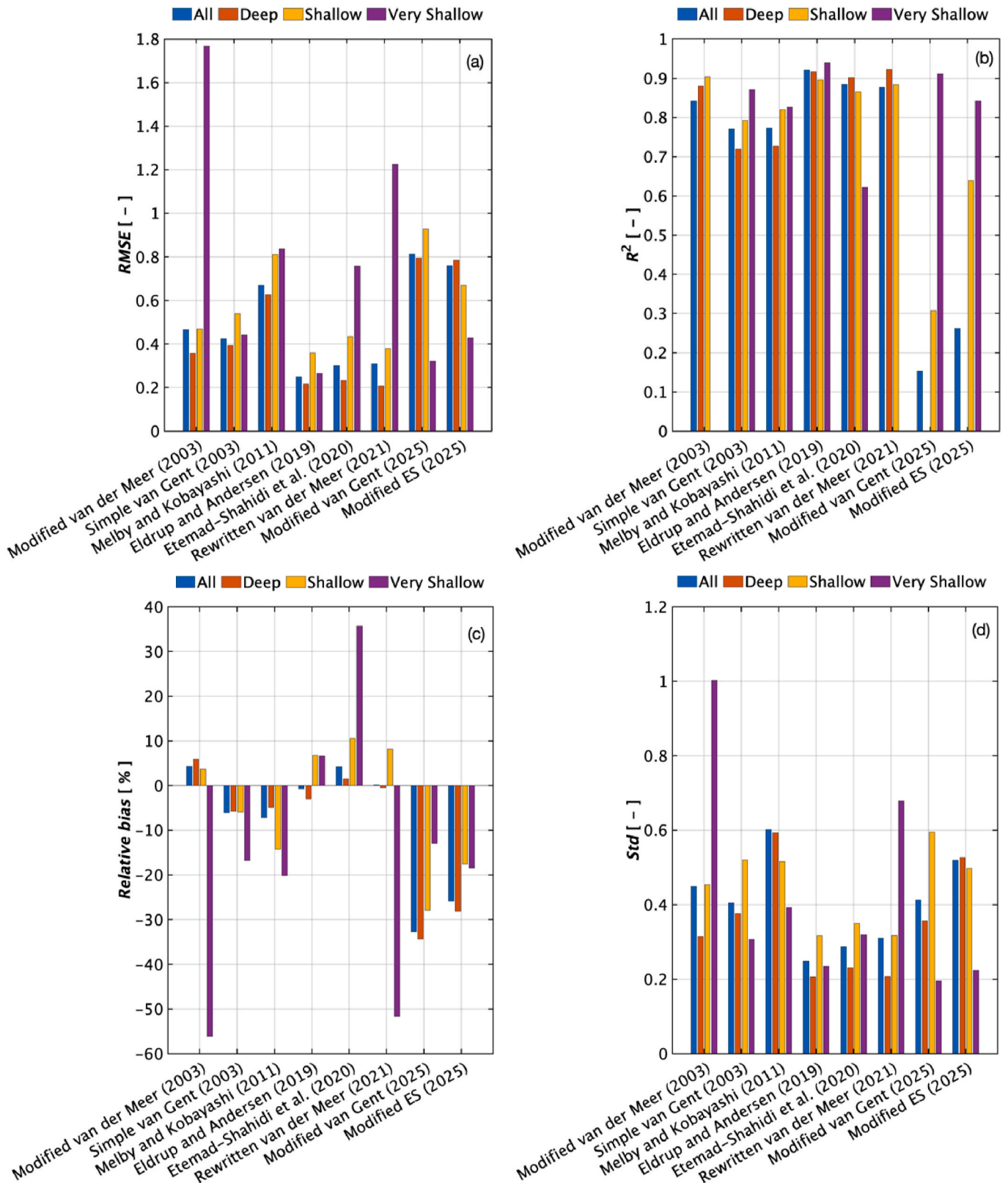


Fig. 7. Bar plot with the error metrics for the stability formulae based on water depth conditions: a) RMSE; b) R^2 ; c) Relative bias; d) Std.

deep water conditions with flat bottoms. Recently, VDM tested the equations outside their intended range of application using VSK and EA datasets, highlighting that equations are valid up to $h/H_{m0,deep} > 1.5$ (van der Meer et al., 2024). In the present study, the equations show good agreement with deep water data, with 18% of data falling outside the

90% confidence bands. For shallow ($0.40 \leq h_r < 1.5$) and very shallow ($h_r \geq 1.5$) water conditions 12% and 29% of the data, respectively, fall outside the 90% confidence bands. Considering the original equations, some of the uncertainty can be attributed to the permeability of the structure, which is represented by the somewhat subjective “notional”

permeability factor (P). During the development of the stability formula, fixed values of P were assigned to represent different stability trends under surging wave conditions, with higher values of P corresponding to steeper stability curves. Moreover, in shallow water conditions, the SSP computed on the structure slope may be less influential than one computed using the foreshore slope for conditions when waves break over a wide surf zone and not directly on the structure slope. Overall, the rewritten VDM stability equations remain applicable for deep water conditions but demonstrate reduced accuracy and increased uncertainty in shallow and very shallow water, emphasizing the importance of considering their range of validity in practical applications.

The Modified van der Meer formula proposed by van Gent et al. (2003) is valid in shallow water but on average exhibits a larger bias and uncertainty compared to the Rewritten VDM equation. This formula was fitted using VDM and VSK datasets under deep and shallow water conditions. Its parameterization is identical to that of Eq. (1a,b), except for the inclusion of $H_{2\%}$. Initially, $H_{1/3}$ was used in the analysis, later $H_{2\%}$, but H_{m0} has now been widely recognized as the suitable wave height in stone armor stability due to its energy-based nature. However, in the shallowest water depths where IG energy becomes dominant, short and long wave energy components could be considered separately (de Ridder et al., 2024), leading to different values for the wave heights and for the wave steepnesses. However, the available data does not allow for such analysis. The Modified van der Meer formula is reasonably accurate for plunging waves but significantly overpredicts stability for surging waves for $h_r \geq 1.5$. This limitation, shared with the Rewritten VDM equation, explains why the formula's accuracy decreases in very shallow water. In such conditions, where waves are continuously breaking and IG waves become influential, the trends in the VDM graphs (SSP vs. combined stability number) tend to become horizontal, exhibiting substantial scatter. This suggests that, under very shallow water conditions, the wave period based on the entire wave spectrum (and therefore the SSP) has a limited influence, or that the energy period based on the entire wave spectrum is not the optimal parameter to use.

The Simple van Gent equation addresses some of the shortcomings of Eq. (2a,b) by employing a simplified formula that excludes the influence of wave period. It incorporates the permeability coefficient, $(1 + D_{n50,core}/D_{n50})$, as a more physically based alternative to the notional permeability factor P . The equation was calibrated using VDM and VSK datasets and exhibits a consistent bias across deep and shallow water when applied to the entire database. The VSK dataset demonstrated that the wave period can increase in shallow water due to energy transfer from swell to IG frequencies. The Simple van Gent equation does not align well with the data in the range $0.4 \leq h_r < 1.5$, primarily because the equation was calibrated using the entire dataset, including conditions outside this range. However, it shows acceptable agreement with the data under very shallow water conditions with 29% of data falling outside the 90% confidence bands.

The Etemad-Shahidi et al. (2020) equation was derived using a multi-variable regression model applied to an experimental database of 791 data available in the literature (VDM, TS, VSK, VML) to develop a compact formula suitable for both plunging and surging waves, valid from deep to shallow water conditions. The formula introduces advancements in a more physically based description of the permeability coefficient $(1 + D_{n50,core}/D_{n50})$, and the inclusion of the foreshore slope parameter $m = \tan\beta$. Additionally, machine learning algorithms revealed a different dependency, showing a 6-power relationship between the stability number and the damage. The transition between plunging and surging waves is defined by $\xi_{s-1,0} = 1.8$ (Battjes, 1974), instead of modeling a continuous transition between these two equations. Overall, the equation shows an increase in bias, which becomes relatively high in very shallow water, while the Std remains relatively constant. The formulation was calibrated with only a limited amount of data in very and extremely shallow water conditions, which causes it to perform less well for very and extremely shallow water. Nevertheless, the ES

equation demonstrates excellent predictive capability for deep water conditions and a reasonably good performance for shallow water conditions, and low uncertainty when applied to the entire database.

The EA equation can be regarded as an updated version of the original VDM. It was calibrated using data with nonbreaking, breaking, and very low steepness waves, incorporating VSK and EA datasets. A significant improvement is the inclusion of highly nonlinear wave data in shallow water (EA dataset), along with the use of the formula by Eldrup et al. (2019) to estimate P (though this specific estimation was not applied in the current comparison). Notably, the EA equation exhibits no influence on wave steepness in the surging domain, which aligns with trends observed in some shallow water datasets, particularly for the steeper slopes. However, the relationship between the stability number and the structure slope in the surging equation seems overly simplistic, as it primarily considers steep armor slopes, excluding milder slopes. The SSP was estimated using wave steepness at the structure toe, calculated from the deep water wavelength formula $gT^2/(2\pi)$, where N_w is considered offshore. This formulation exhibits a relatively low increasing bias from deep to shallow water, with 11% data falling outside the 90% confidence bands for shallow water and only 5% data for very shallow water. Its similarity to the VDM equation also supports accurate prediction in deep water, although Eq. (6a,b) was not explicitly calibrated with VDM data. Among the tested formulations, the EA equation presents low values of bias and uncertainty in shallow and very shallow water. This can be attributed to its calibration using homogeneous datasets acquired in recent years (similar technologies compared to the 1980s). Different hydrodynamic and damage measurements and analyses between the experiments can explain the residual bias. Importantly, the uncertainty in the EA equation remains relatively constant across all water depth conditions, indicating robust predictive performance. A difference with the previous formulae is that they used EA data with cumulative damage (not rebuilding the armour after every test) and applied different P -values for permeable core structures. This makes it challenging to compare directly with other formula. Overall, the EA equation demonstrates good/best performance across all water depth conditions, achieving small $RMSE$, μ , Std , PSE and high R^2 values. However, the EA formula does not perfectly match some VSK and EUMER data in shallow water. As for VSK data, EA stated that this discrepancy may result from the limited VSK data available in the surging domain, as other data were generated outside the range of what they consider valid for second-order wavemaker theory (Eldrup et al., 2019).

The MK equation is theoretically expected to perform better than the other formulations, since it is more physically based and analytically derived from basic principles. This equation utilized the maximum depth-integrated wave momentum flux $(M_f)_{max}$ to characterize wave forces on the structure and explicitly incorporates the local water depth. Eq. (4a,b) was calibrated utilizing only the VDM dataset in deep water conditions (Melby and Kobayashi, 2011). Despite these theoretical advancements, the results presented in Fig. 6c reveal suboptimal but not worse performance compared to the better models. Bias increases as relative depth increases, which can be attributed to the mixing of non-homogeneous data as well as the limited amount of shallow water data used to calibrate this formula. Nevertheless, the uncertainty associated with the MK equation remains relatively constant, suggesting that the formulation accurately captures the underlying physical processes. The observed uncertainty may partly stem from the approximation of the nonlinear $(M_f)_{max}$ at the structure toe, rather than its precise computation at the upslope location where the maximum forces occur (Hughes, 2004). This approximation breaks down, especially under nonlinear breaking conditions.

The Modified van Gent and the Modified ES equations were calibrated exclusively using the EUMER dataset and have proven effective in very and extremely shallow water conditions. However, they exhibit significant bias in both deep and shallow water conditions compared

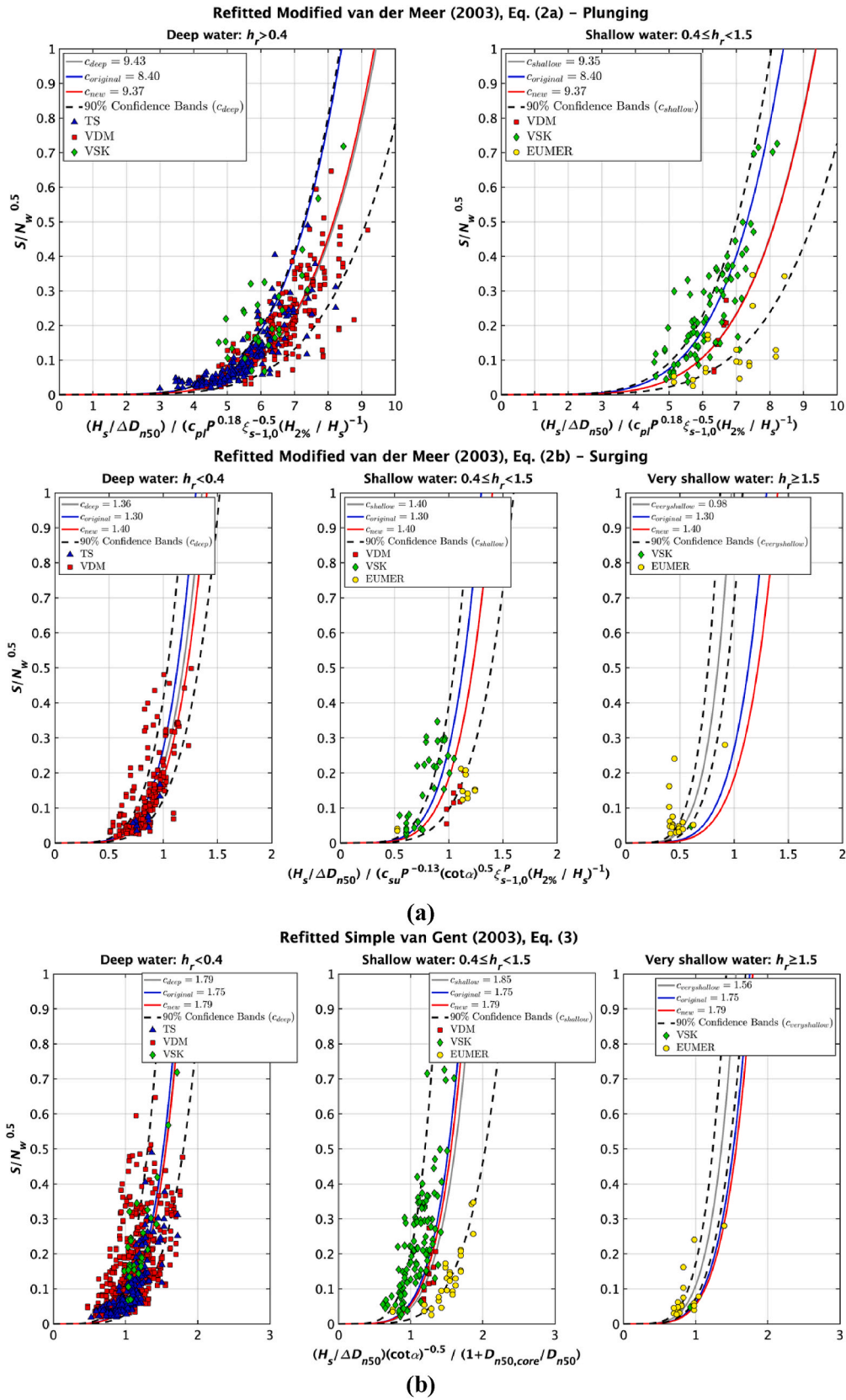


Fig. 8. Refitting of stability equations for deep (left), shallow (center) and very shallow (right, if data are available) water: a) Modified van der Meer (2003) (van Gent et al., 2003); b) Simple van Gent (2003) (van Gent et al., 2003); c) Melby and Kobayashi (2011); d) Eldrup and Andersen (2019); e) Etemad-Shahidi et al. (2020); f) Rewritten van der Meer (2021) (van der Meer, 2021); g) Modified van Gent (2025) (Scaravaglione et al., 2025); h) Modified ES (2025) (Scaravaglione et al., 2025).

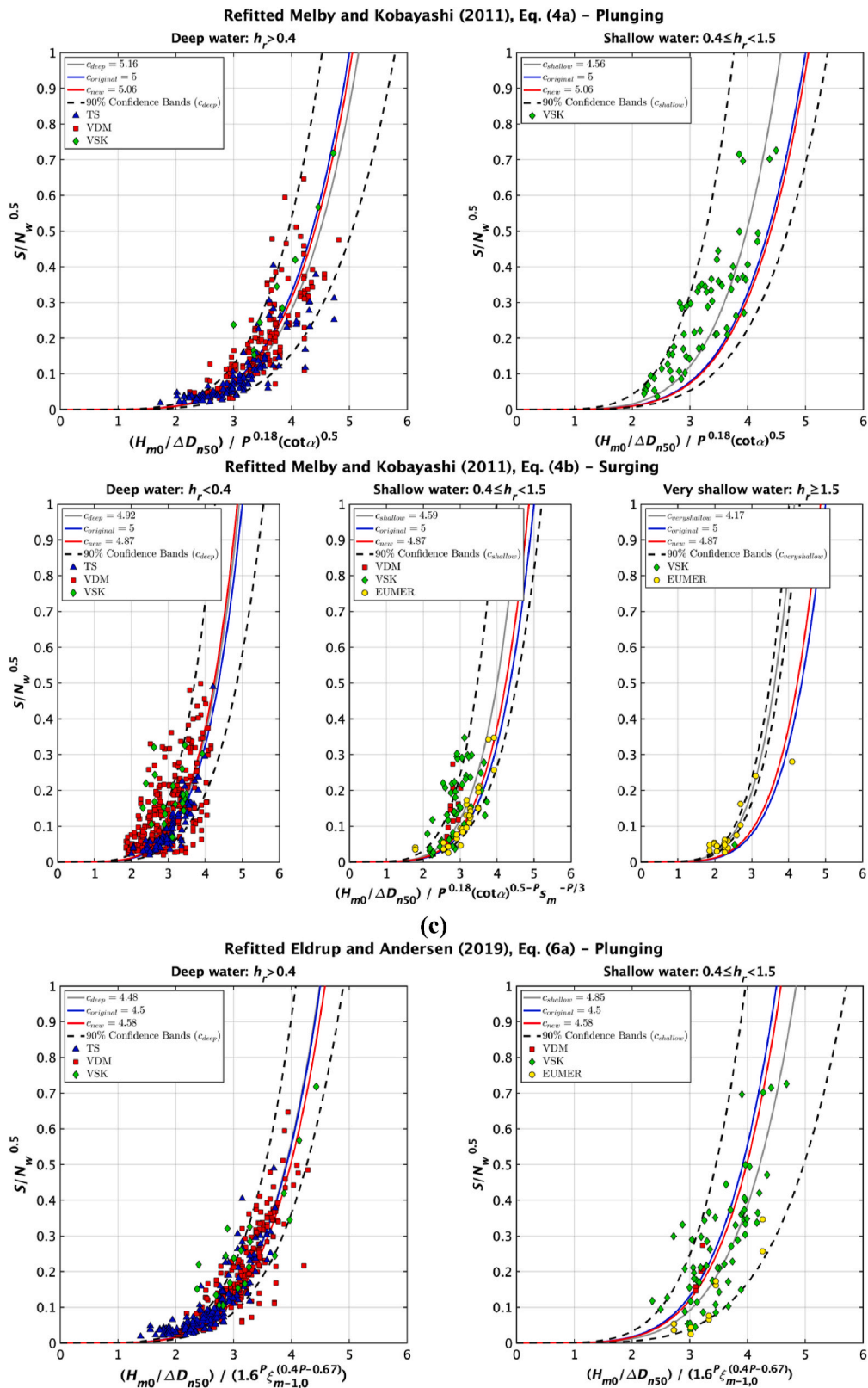


Fig. 8. (continued).

with other datasets. These equations were developed to investigate the influence of shallow water on stone armor stability, utilizing the only available dataset in very shallow water. They represent an adaptation of the Simple van Gent equation (van Gent et al., 2003) and the ES equation (Etemad-Shahidi et al., 2020), focusing exclusively on

depth-limited data and incorporating wave steepness into the predictive model to account for the effect of shallow water. The substantial bias observed in shallow water, particularly between VSK and EUMER datasets, is likely attributable to the inherent uncertainty present in the laboratory data of these two distinct datasets. Despite their limitations,

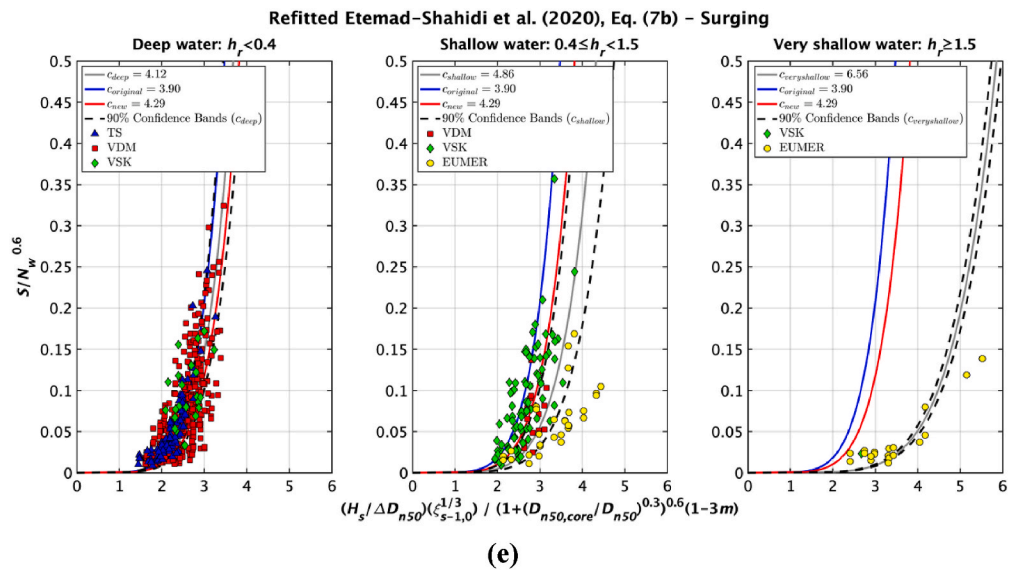
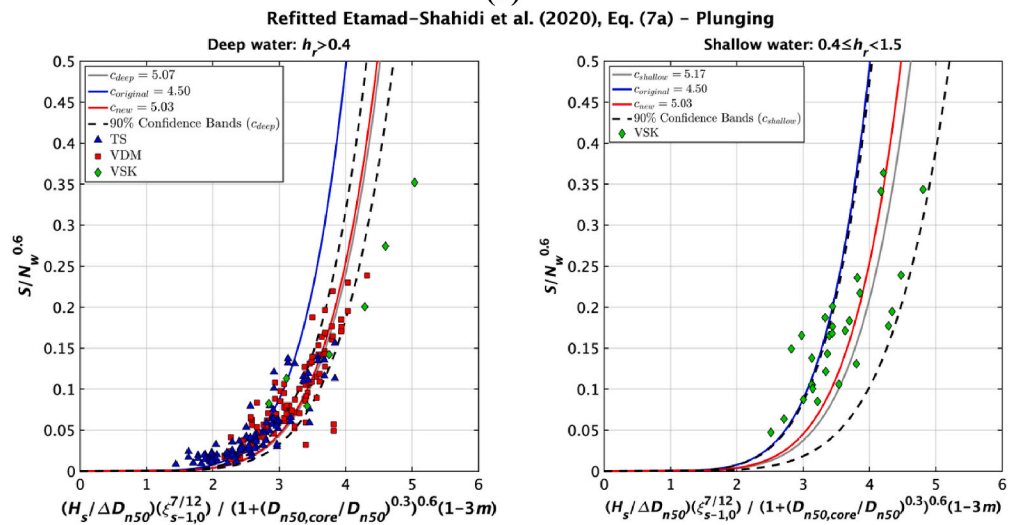
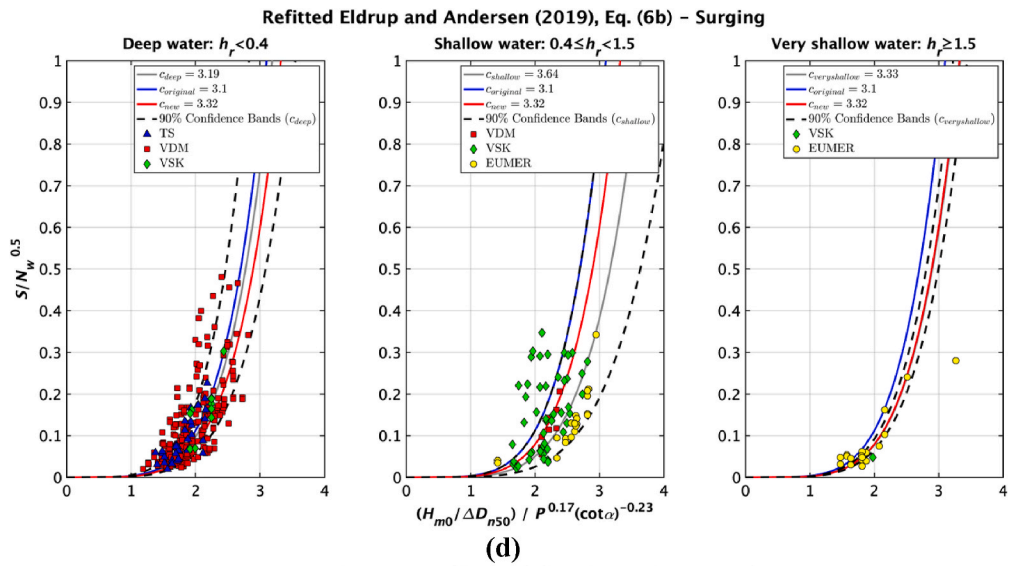


Fig. 8. (continued).

the Modified van Gent and Modified ES equations (Scaravaglione et al., 2025) as well as the EA equation appear as relatively reliable methods to describe stone armor stability in very shallow water conditions ($h_r \geq 1.5$).

Among the equations analyzed, the Rewritten VDM, EA and ES equations exhibit good agreement for deep water conditions. However, the Rewritten VDM and ES equations tend to perform worse in shallow

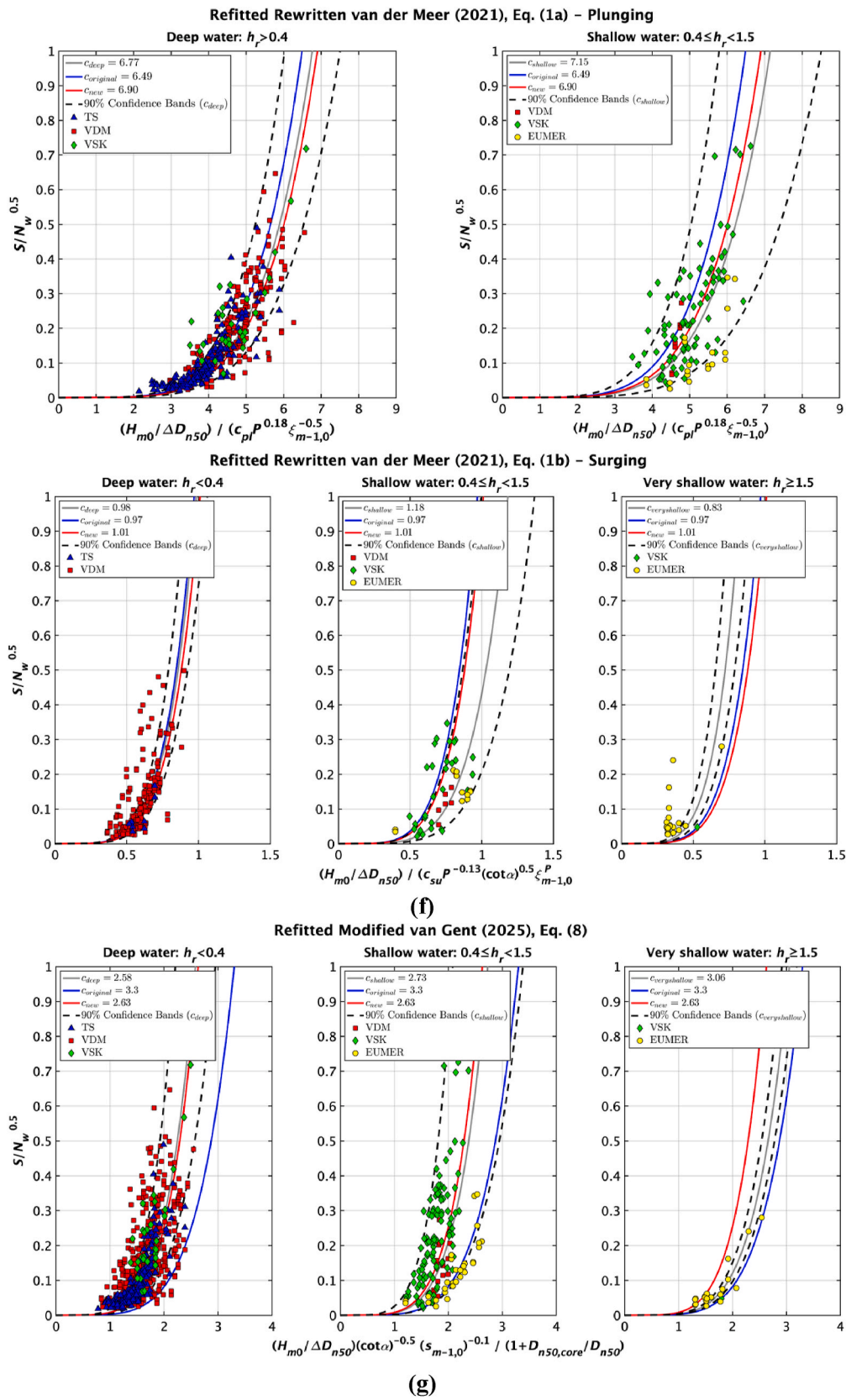


Fig. 8. (continued).

and very shallow water compared to their performance in deep water, suggesting missing elements in these formulations for such conditions. Indeed, while EA and the Rewritten VDM still perform reasonably well

in shallow water ($0.4 \leq h_r < 1.5$), they require adjustments to reduce bias, as these equations were not calibrated for the present comprehensive database. For very shallow water ($h_r \geq 1.5$), the Modified van Gent,

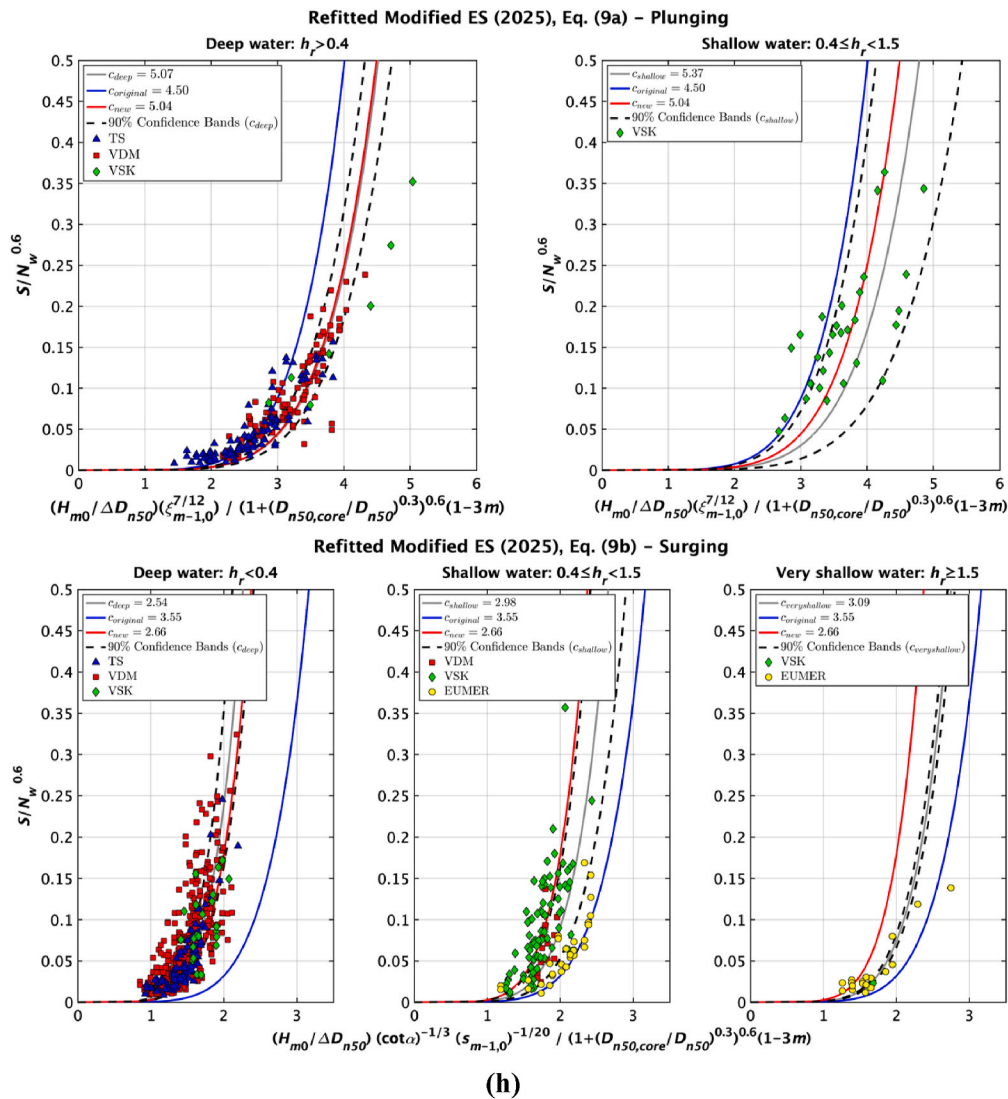


Fig. 8. (continued).

Modified ES and EA equations prove to be more effective and accurate than the others. This supports the conclusion that, in very shallow water, the influence of the wave steepness on armor stability is present but relatively minor. Consequently, simpler equations may be more appropriate for these conditions. In very shallow water with a wide surf zone, it is speculated that the details of wave-to-wave variations and their influence on stability are reduced due to breaking and energy saturation. If this holds true, it suggests that both the VDM functionality and epistemic variability diminish under such conditions. Furthermore, in wide surf zones, many parameters that are influential in deep water may not exert much influence. This raises an important question: is epistemic uncertainty dependent on factors such as the relative depth and width of the surf zone, or does it primarily result from one set of factors in deep water and another set in shallow water? A definitive answer to this question cannot be provided until epistemic uncertainty is further reduced. For now, we can only speculate and rely on the literature to identify the primary sources of bias and uncertainty. Discrepancies between various sources of data may potentially arise from experimental factors, such as difference between the use of active compensation reflection system, 2nd order wave generation techniques, reflection analysis methods, calibration tests with and without the structure, position of the wave gauges near the toe of the structure, as well as

variations in damage profiling and profile analysis procedures.

3.3. Refitting of stability equations using the new database

This section presents a recalibration of the stability formulae introduced in Section 1, leveraging the newly comprehensive database to derive updated regression coefficients, hereafter denoted as ‘c’, and to quantify uncertainty across different formulation and water depth condition. The stability equations are refitted using a nonlinear optimization method that minimizes the sum of the squared residuals between observed and predicted values. To ensure robust coefficient estimates, a bootstrapping technique is employed. Each regression is iterated 150 times using randomly resampled datasets, each comprising 80% of the total database (0.80M) drawn from a database of size M. Consequently, individual data points may appear multiple times within a given bootstrap sample or may be entirely absent. The final best-estimate coefficient (c) is determined as the mean of the bootstrapped parameter distribution. To mitigate the influence of extreme deviations, a local control technique is applied to identify and remove high-error data points classified as outliers. Outliers are detected using the interquartile range (IQR) method, with an exclusion threshold set at three standard deviations. This approach ensures a more reliable coefficient estimation

Table 7
Main errors metrics of the refitted stability equations compared in Fig. 8.

Stability Formulae		Original - All				Refitted - All				Refitted - Deep				Refitted - Shallow				Refitted - Very Shallow			
		$c_{original}$	RMSE	R^2	CoV	c_{new}	RMSE	R^2	CoV	c_{deep}	RMSE	R^2	CoV	$c_{shallow}$	RMSE	R^2	CoV	$c_{veryshat.}$	RMSE	R^2	CoV
		[-]	[-]	[-]	[%]	[-]	[-]	[-]	[%]	[-]	[-]	[-]	[%]	[-]	[-]	[-]	[%]	[-]	[-]	[-]	[%]
Mod. VDM (2003)	Plunging	8.4	0.156	<0	140	9.37	0.088	0.47	148	9.43	0.072	0.54	148	9.35	0.088	0.47	149	Nan	Nan	Nan	Nan
	Surging	1.30	0.109	<0	156	1.4	0.091	0.12	147	1.36	0.075	0.42	162	1.40	0.091	0.12	146	0.98	0.071	<0	133
Simple van Gent (2003)		1.75	0.117	<0	141	1.79	0.115	<0	134	1.79	0.104	<0	137	1.85	0.173	<0	116	1.56	0.053	<0	133
MK (2011)	Plunging	5	0.100	0.46	149	5.06	0.099	0.47	147	5.16	0.076	0.59	151	4.56	0.116	0.52	116	Nan	Nan	Nan	Nan
	Surging	5	0.087	0.13	124	4.87	0.085	0.17	134	4.92	0.085	0.21	134	4.59	0.084	<0	126	4.17	0.021	0.83	127
EA (2019)	Plunging	4.5	0.074	0.62	151	4.58	0.072	0.64	138	4.48	0.058	0.73	147	4.85	0.112	0.50	126	Nan	Nan	Nan	Nan
	Surging	3.10	0.098	<0	145	3.32	0.081	0.16	140	3.19	0.071	0.39	140	3.64	0.095	<0	134	3.33	0.020	0.84	125
ES (2020)	Plunging	4.50	0.090	<0	147	5.03	0.035	0.60	123	5.07	0.031	0.61	117	5.17	0.087	<0	103	Nan	Nan	Nan	Nan
	Surging	3.90	0.074	<0	159	4.29	0.049	0.16	128	4.12	0.041	0.37	131	4.86	0.066	<0	116	6.56	0.014	0.13	100
Rewr. VDM (2021)	Plunging	6.49	0.104	0.17	160	6.90	0.082	0.48	140	6.77	0.069	0.59	145	7.15	0.117	0.39	131	Nan	Nan	Nan	Nan
	Surging	0.97	0.067	0.40	145	1.01	0.059	0.52	133	0.98	0.050	0.65	140	1.18	0.101	<0	123	0.83	0.061	<0	119
Mod. van Gent (2025)		3.30	0.147	<0	88	2.63	0.103	0.17	139	2.58	0.091	0.23	145	2.73	0.152	<0	127	3.06	0.028	0.12	124
Mod. ES (2025)	Plunging	4.50	0.090	<0	143	5.04	0.034	0.63	123	5.07	0.031	0.61	117	5.37	0.092	<0	101	Nan	Nan	Nan	Nan
	Surging	3.55	0.076	<0	80	2.66	0.048	0.17	132	2.54	0.041	0.36	138	3.00	0.059	<0	125	3.09	0.011	0.40	110

*Colored legend for performance: green = high R^2 ($R^2 \geq 0.40$), yellow = mid R^2 ($0.2 \leq R^2 < 0.4$), orange = low R^2 ($R^2 < 0.2$). Green = low RMSE ($RMSE < 0.05$), yellow = mid RMSE ($0.05 \leq RMSE < 0.10$), orange = high RMSE ($RMSE \geq 0.10$). Green = low CoV ($CoV < 100$), yellow = mid CoV ($100 \leq CoV < 140$), orange = high CoV ($CoV \geq 130$).

while minimizing data loss, thereby preserving the integrity of the central fits and effectively eliminating extreme deviations. However, a key limitation of this analysis is that the original formulations remain unchanged.

Fig. 8 illustrates the corresponding stability curves, where $S/\sqrt{N_w}$ is plotted along the vertical y-axis, comparing the original regression lines (blue) with the newly derived regression lines (red), obtained considering all data. Additionally, newly derived regression lines for deep, shallow, and very shallow water conditions are presented in grey. Assuming a Gaussian error distribution, the uncertainty of the refitted stability formulae is described with a 90% confidence interval lines (dotted black) given by Eq. (12):

$$S_d|_{5\%}^{95\%} = S_{best-estimate} \pm 1.64Std \tag{Eq. 12}$$

where S_d is the design value and $S_{best-estimate}$ is given by the refitted stability equations.

It is important to note that for plunging conditions, very shallow water data are absent; consequently, the corresponding plots are not included. Furthermore, RMSE, R^2 , and CoV values were calculated for each stability curve and serve as indicators of total error and uncertainty, encompassing both intrinsic and epistemic uncertainties, as summarized in Table 7. The comparison of the refitted stability equations provides valuable insights into the predictive capabilities of different models, given that all equations have been calibrated using a common database. However, it is important to clarify that the RMSE and R^2 reported in Table 7 are not directly comparable to those in Table 5. This discrepancy arises from the different methodological approaches employed: Table 5 is based on a combined analysis of plunging and surging waves using the stability number (N_s), whereas Table 7 presents results from a separate analysis for plunging and surging waves, based on the normalized damage parameter ($S/\sqrt{N_w}$). Accordingly, any

variation in RMSE and R^2 reflects the distinct response variables and grouping strategies applied. To improve clarity and facilitate direct comparison with the original formulations shown in Fig. 6 and Table 5, additional supplementary materials have been included in Appendix A, comprising a supplementary figure (Fig. A9) and table (Table A8) reporting the corresponding error metrics for the refitted equations expressed in terms of the stability number (N_s).

3.4. General discussion on uncertainty in stone armor stability

This section discusses the uncertainty associated with stone armor stability, based on the results outlined in Section 3.2 and summarized in Table 7. Mathematically, “uncertainty” is mainly defined as the relative variation of a statistical parameter or relative error in the model description. The accuracy of such estimates depends on the quality and comprehensiveness of the database, which should be derived, as in the present study, from different tests, measurements, and investigations. Indeed, forming a robust and extensive database is highly desirable, as it facilitates research efforts aimed at improving the predictive accuracy of the empirical formulations. Nevertheless, assessing the statistical nature of errors in coastal engineering remains challenging due to the presence of multiple sources of uncertainty and the inherent non-homogeneity of available datasets. In the present study, uncertainty is quantified using two complementary metrics: the Root Mean Square Error (RMSE) and the Coefficient of variation (CoV), as defined in Eqs. (10a,e). Indeed, due to the nature of the data representation in Fig. 7, which compares predicted vs. measured normalized damage ($S/N_w^{0.5}$), the data exhibit considerable scatter. This high degree of variability often results in low or even negative values of the coefficient of determination (R^2), highlighting a well-known limitation of this metric when applied to highly dispersed data. In such contexts, R^2 may lose interpretability and offer

limited insight into model performance. For this reason, R^2 was not considered in the subsequent discussion of predictive capability.

Among the evaluated stability formulations, the refitted ES and Modified ES equations exhibits the lowest *RMSE* values (0.035/0.034 for plunging and 0.049/0.048 for surging), outperforming all other models in overall predictive accuracy. Specifically, the *RMSE* values for the refitted models are nearly half of those obtained for the other stability equations, demonstrating better performance across varying water depth conditions. When considering the coefficient of variation as a measure of relative uncertainty, the ES and Modified ES formulae also demonstrate the lowest *CoV* values across the entire dataset, with 123% for plunging and 128/132% for surging waves. This indicates enhanced predictive consistency across deep, shallow, and very shallow water conditions. While other stability equations exhibit comparable *CoV* values, they are often associated with higher *RMSE* values than those of the ES and Modified ES formulae, highlighting a fundamental trade-off between minimizing predictive error and reducing uncertainty across diverse hydrodynamic conditions.

To further delineate refitted model performance across specific depths, a category-wise assessment is provided below:

- **Deep water:** The refitted ES and Modified ES formulae yield the lowest *RMSE* values (0.031 for plunging and 0.041 for surging) while maintaining a moderate *CoV* (117% for plunging and 131/138% for surging). The third-best performing model for plunging waves is the EA equation, with an *RMSE* of 0.058 (*CoV*=147%). For surging waves, the Rewritten VDM formula achieves an *RMSE* of 0.050 (*CoV*=140%). The Simple van Gent model, despite exhibiting a relatively low *CoV* (137%), presents a considerably higher *RMSE* (0.104). Nevertheless, it remains a valid alternative due to its inherent continuity between plunging and surging, as well as its simplicity.
- **Shallow water:** The refitted ES and Modified ES formulae continue to demonstrate superior performance, yielding the lowest *RMSE* values (0.087/0.092 for plunging and 0.066/0.059 for surging) alongside the lowest *CoV* values (103/101% for plunging and 116/125% for surging). The third-best performance for plunging waves is observed in the Modified VDM, which exhibits an *RMSE* of 0.088 and a *CoV* of 149%. For surging waves, the MK formula ranks third, with an *RMSE* of 0.084 and a *CoV* of 126%. The Simple van Gent equation also maintains a relatively low *CoV* (116%), further reinforcing its stability in predictive outcomes.
- **Very Shallow water:** The refitted ES and Modified ES formulae sustain their trend of superior performance, achieving the lowest *RMSE* (0.014/0.011) and *CoV* (100/110%) for surging waves. The EA and MK equations follow closely, with *RMSE* values of 0.020 (*CoV*=125%) and 0.021 (*CoV*=127%), respectively. The Modified van Gent model also exhibits competitive performance, achieving an *RMSE* of 0.028 and a *CoV* of 124%. This outcome is largely due to its simplified formulation and the fact that it was calibrated using nearly the entire dataset for very shallow water.

Overall, the refitted ES and Modified ES stability formulae consistently demonstrate superior predictive performance across all analyzed statistical metrics and water depths. However, despite their apparent advantages, the damage plots still reveal substantial uncertainties persisting across all examined conditions. Each of the examined equations presents distinct strengths and weaknesses, and the choice remains debatable, primarily due to the inherent variability and limitations associated with laboratory-generated datasets. The relatively high *CoV* values for all models highlight the persistent challenge of accurately capturing the complex relationships between hydrodynamic forces and structural response, since significant uncertainties remain intrinsic within existing predictive frameworks, potentially obscuring the fundamental physics governing stone armor stability.

These findings have practical implications for design practice,

particularly by informing the selection and calibration of stability formulae under varying hydrodynamic conditions. While this study does not recommend a specific formulation for design purposes, due to the inherent limitations and variability of the data, it provides estimates of the coefficient of variation (*CoV*) associated with both original and refitted best estimate coefficients for varying shallowness conditions. For practical applications, designers may adopt the equation and corresponding coefficients that best align with project-specific conditions, or alternatively, apply a conservative approach by selecting the worst-case coefficient(s) across all water depth regimes. The final choice should be guided by the project's performance criteria and risk tolerance. To account for uncertainty, it is advisable to select coefficients corresponding to a predefined confidence level (CL), such as the 90% CL illustrated in Fig. 8. This method does not rely solely on the best-fit regression, but instead utilizes a curve specifically designed to reduce the risk of underestimation of damage. In a standard stability plot, the best-estimate curve can be considered representative of the 50th percentile response within the range $1 \leq S \leq 1.5S_{\max}$. However, it is important to apply the equations only within the design range specified in Table 2. The decision to pursue a fully probabilistic Monte Carlo simulation or a semi-deterministic approach incorporating frequency-based inputs (e.g., 50-year average recurrence interval) remains highly site-specific and should consider both local environmental context and client/contractor requirements.

The results underscore the complexity of the topic and the challenges associated with developing a universally robust stability equation. Besides being important to emphasize that most stability equations are empirical or semi-empirical in nature, designed to fit specific wave and water level conditions, further difficulties stem from the technological evolution in measurement techniques. Deep water data often originate from older measurement methodologies, whereas shallow water data are typically derived from more advanced, modern instrumentation. This contrast introduces potential biases and systematic offsets between datasets, complicating direct comparison. Without further analysis, it remains difficult to ascertain which sources of uncertainty are most influential. This study highlights the need for a more rigorous treatment of incident wave spectra in shallow water, a critical but often neglected aspect of stability analyses. Laboratory-specific phenomena, such as low-frequency waves, combined with challenges in measuring and analyzing reflected waves, add substantial variability, particularly in shallow water. Consequently, even under ostensibly similar technical conditions, physical model studies on hydrodynamics and damage analysis exhibit intrinsic variability and, hence, the above discussed uncertainties which have to be systematically integrated into the design of coastal structures.

4. Conclusions

The present study presents a detailed analysis of stone armor stability, comparing a new damage database (691 tests) with widely used stability equations to evaluate accuracy and quantify uncertainty across different shallowness conditions. Existing experimental data in the literature have been examined and synthesized, leading to the formation of a new database encompassing varied water depths from deep to very shallow water conditions (h_r up to 5). Data synthesis was accomplished by collecting and homogenizing data from 4 different international studies considering the disparate nature of the original data. Benefiting from this extensive database, the established armor stability formulae i. e., Modified van der Meer (2003) (van Gent et al., 2003), Simple van Gent (2003) (van Gent et al., 2003), Melby and Kobayashi (2011), Eldrup and Andersen (2019), Etemad-Shahidi et al. (2020), Rewritten van der Meer (2021) (van der Meer, 2021), Modified van Gent (2025) (Scaravaglione et al., 2025), Modified ES (2025) (Scaravaglione et al., 2025) were compared within the framework of quantifying uncertainty and allowing for a systematic comparison of the original and refitted equations across all water depths. The refitted ES and Modified ES

stability equations exhibit lower *RMSE* and *CoV* values when compared in the typical predicted vs. measured normalized damage plot. Each formulation presents strengths and weaknesses, with predictive accuracy varying across hydrodynamic regimes. One key limitation of this study is the dominance of deep water data in the dataset, which may introduce biases when computing bulk statistical metrics across all depth regimes. For this reason, data were divided into deep, shallow, and very shallow water regions and separate equation fitting was reported. Still, the current approach aggregates data without weighting, which can lead to an overrepresentation of deep water conditions.

In conclusion, results are nuanced, and significant uncertainties remain inherent in existing stability equations, reflecting both the variability in experimental datasets and the limitations of empirical and semi-empirical formulations. The refitting of the formulae clearly enhances predictive accuracy in some contexts, but it does not eliminate the fundamental challenges associated with stone armor stability modeling which is affected by both aleatory and epistemic uncertainties. Aleatory uncertainty, arising from the intrinsic randomness of wave conditions, stone placement, and material properties is irreducible. Conversely, epistemic uncertainty originates from limitations in models, measurement techniques, and physical understanding, and can be mitigated through improved knowledge and enhanced experimental methodologies. Distinguishing between epistemic and intrinsic uncertainty, as well as the quantification and separation of their relative proportions to the total uncertainty, presents a complex challenge. The intricate relationship between model and data uncertainties adds another layer of complexity. To tackle this challenge and enhance the overall capabilities of the predictive models, a primary focus should be on improving data accuracy and reliability through standardized procedures, consistent methodologies, and enhanced data quality.

The present study aims to address such a challenge without presuming to solve it completely. There is evidence that variations in experimental methodologies can yield divergent test results, potentially leading to different design decisions. Achieving standardization in testing procedures to the extent where every laboratory produces identical results is an elusive goal. Intuition and engineering judgment will inevitably differ and remain a major factor in the decision-making process accompanying laboratory test designs. Nonetheless, there is a pressing need to standardize wave parameter definitions and the methods employed for their measurement and computation. This standardization effort holds the potential to alleviate many disparities, thereby reducing bias and uncertainty in the final equations. It is proposed that merely attributing apparent discrepancies in results to normal statistical variability is no longer adequate. Instead, there is a need to learn from this comparative analysis and actively work toward minimizing the epistemic uncertainty inherent within laboratory data. Even in cases where uncertainty cannot be minimized, it must be rigorously assessed to determine whether it falls within acceptable design thresholds. Incorporating probabilistic methodologies into predictive models can help strike a balance between under-design and excessive conservatism, ensuring that coastal defenses are both resilient

and economically viable. In addition, generating data over the entire range from deep water conditions to extremely shallow water conditions using the same wave generation, active reflection compensation, wave separation technique, and damage measurements, may reduce the influence of uncertainties in derived stability expressions based on such a homogeneous dataset.

Future research should aim to extend the analysis toward three-dimensional stability behavior, with particular focus on oblique wave attack (van Gent and Wolters, 2018; Bali et al., 2023) and short-crested wave conditions (Burcharth et al., 2010; Maciñeira and Burcharth, 2016), which remain poorly understood despite their critical relevance to real-world coastal environments.

CRediT authorship contribution statement

Giulio Scaravaglione: Writing – review & editing, Writing – original draft, Visualization, Validation, Supervision, Methodology, Investigation, Formal analysis, Data curation, Conceptualization. **Jeffrey A. Melby:** Writing – review & editing, Writing – original draft, Visualization, Validation, Supervision, Methodology, Investigation, Formal analysis, Data curation, Conceptualization. **Giuseppe R. Tomasichio:** Writing – review & editing, Writing – original draft, Visualization, Validation, Supervision, Methodology, Investigation, Formal analysis, Data curation, Conceptualization. **Marcel R.A. van Gent:** Writing – review & editing, Writing – original draft, Visualization, Validation, Supervision, Methodology, Investigation, Formal analysis, Data curation, Conceptualization. **Alessandra Saponieri:** Writing – review & editing, Writing – original draft, Visualization, Validation, Supervision, Project administration, Methodology, Investigation, Funding acquisition, Formal analysis, Data curation, Conceptualization.

Declaration of competing interest

The authors declare the following financial interests/personal relationships which may be considered as potential competing interests: Co-author Marcel R.A. van Gent is Editor-in-Chief of Coastal Engineering. The manuscript has been handled by one of the associate editors, who selected the reviewers and evaluated the manuscript without any influence on these decisions by the Editor-in-Chief. If there are other authors, they declare that they have no known competing financial interests or personal relationships that could have appeared to influence the work reported in this paper.

Acknowledgments

This work was funded by Piano Nazionale di Ripresa e Resilienza (PNRR), Missione 4 Istruzione e Ricerca, Componente C2, Investimento 1.1 Fondo per il Programma Nazionale di Ricerca e Progetti di Rilevante Interesse Nazionale (PRIN), Research project A PRObabilistic fraMEwork for coasTal and harbor dEfense in the cONtext of climate change, PROM-ETEO (P20224T9SK).

Appendix A. Comparison between observed and refitted predicted stability number

Fig. A9 illustrates the observed vs. predicted stability number (N_s) for each refitted equation, presented separately for deep (left), shallow (center), and very shallow (right) water conditions. For each graph, the 90% confidence bands are reported providing a visual representation of the uncertainty range. The accuracy of the predictions was quantified using standard error metrics (*RMSE*, R^2 , *PSE*, μ , *Std*) and results are presented in Table A8, allowing for a comparison between original and refitted equations.

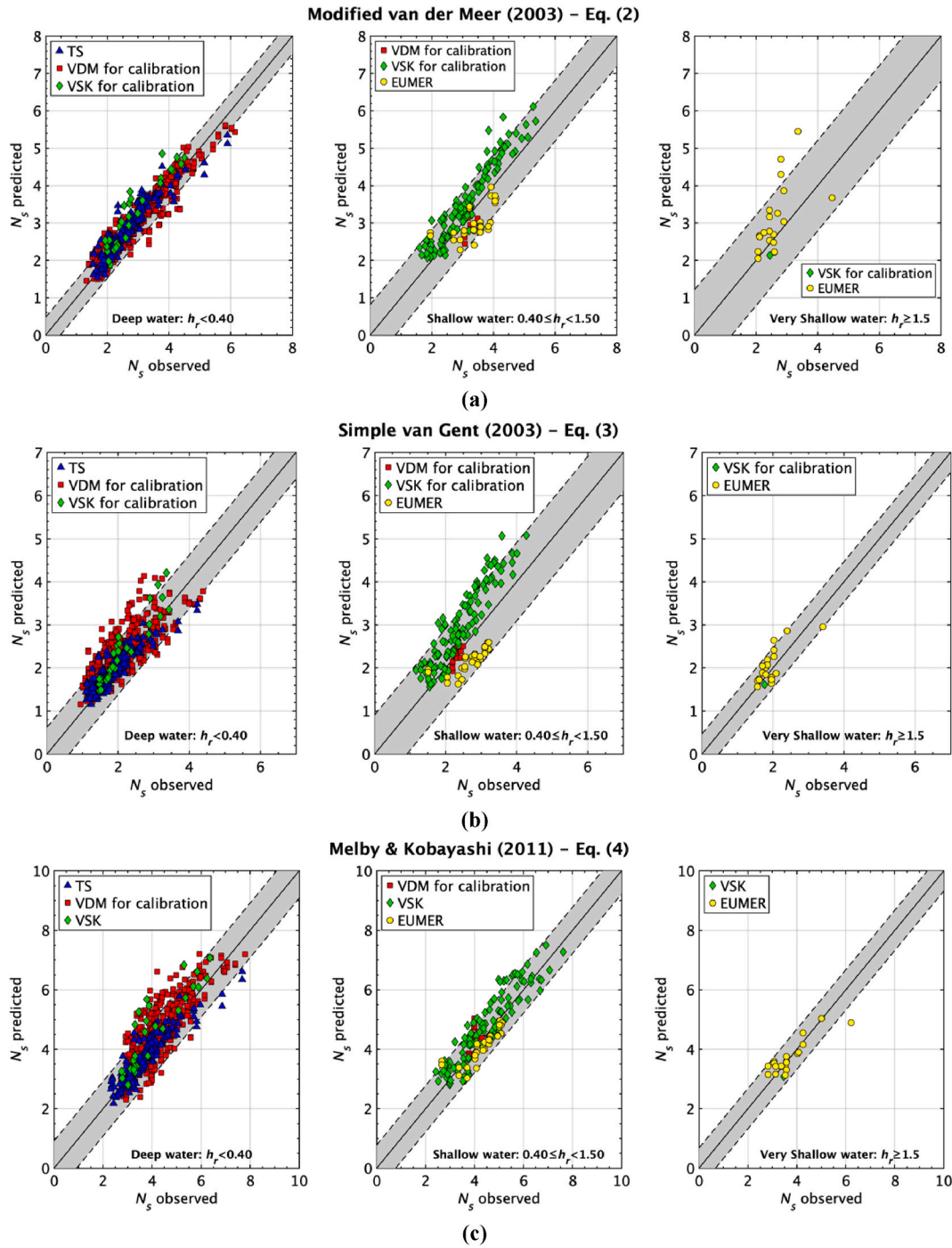


Fig. A9. Comparison between observed and refitted predicted stability numbers by: a) Modified van der Meer (2003) (van Gent et al., 2003); b) Simple van Gent (2003) (van Gent et al., 2003); c) Melby and Kobayashi (2011); d) Eldrup and Andersen (2019); e) Etemad-Shahidi et al. (2020); f) Rewritten van der Meer (2021) (van der Meer, 2021); g) Modified van Gent (2025) (Scaravaglione et al., 2025); h) Modified ES (2025) (Scaravaglione et al., 2025).

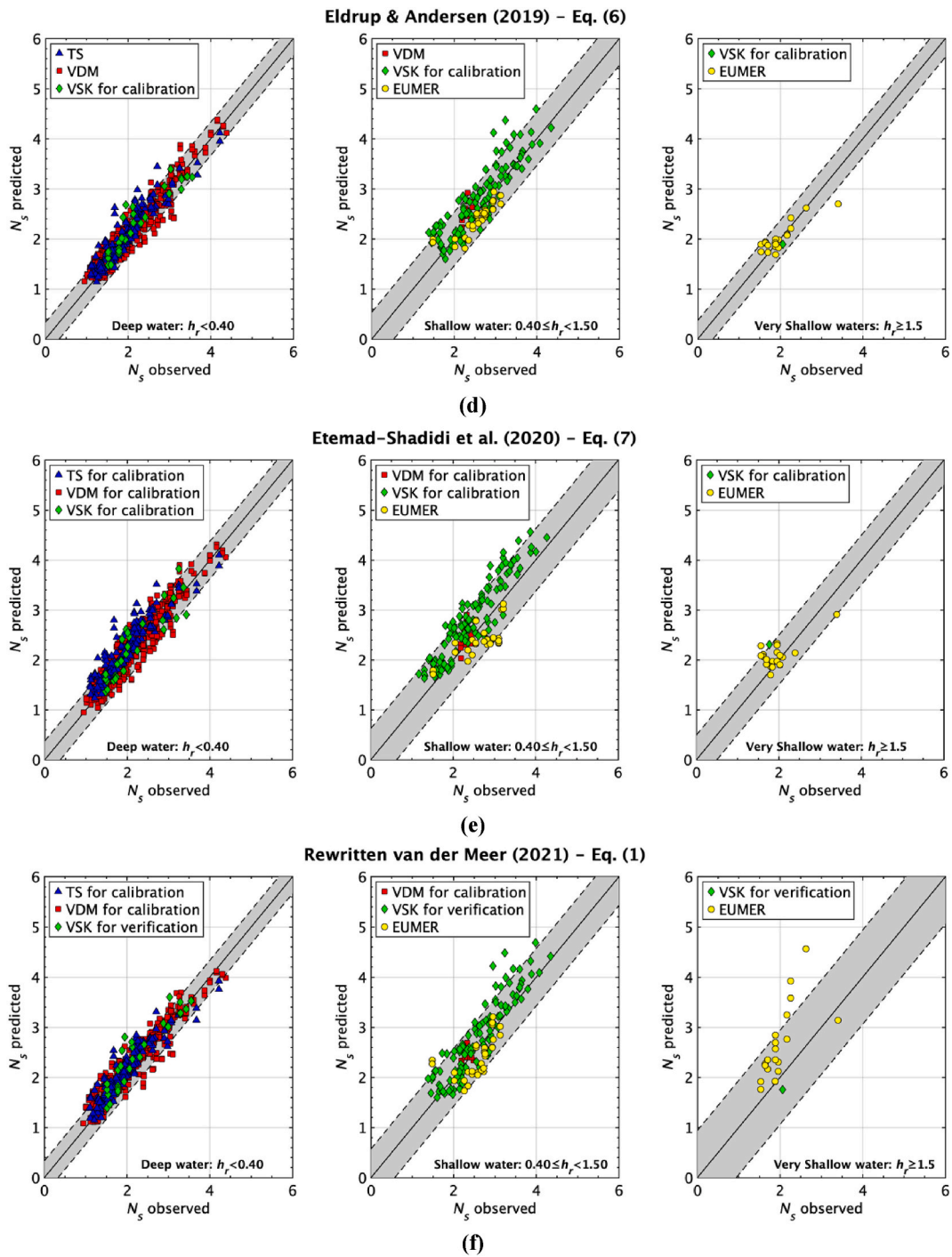


Fig. A9. (continued).

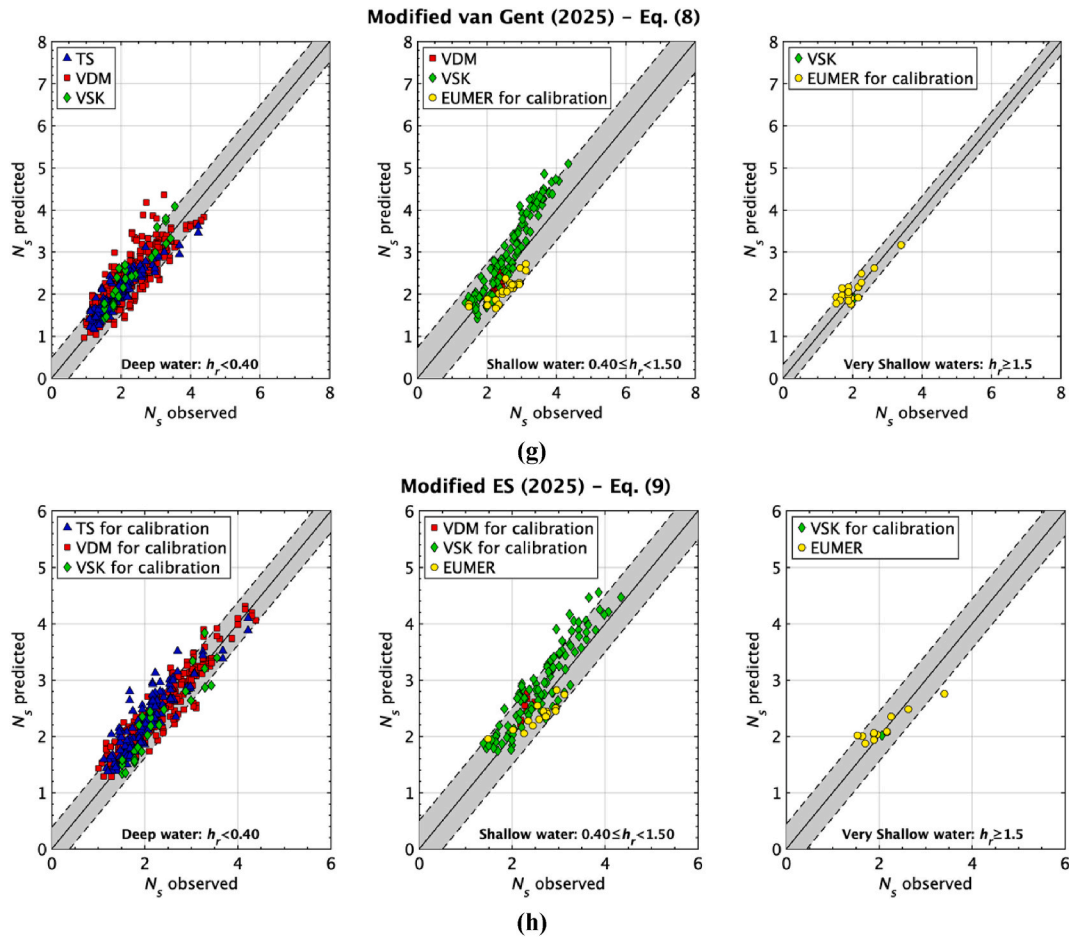


Fig. A9. (continued).

Table A8
Error metrics for refitted stability equations across varying shallowness conditions.

Stability Formulae		Refitted All				Refitted Deep				Refitted Shallow				Refitted Very shallow			
		<i>c_{new}</i>	<i>RMSE</i>	<i>R²</i>	<i>PSE</i>	<i>c_{deep}</i>	<i>RMSE</i>	<i>R²</i>	<i>PSE</i>	<i>c_{shallow}</i>	<i>RMSE</i>	<i>R²</i>	<i>PSE</i>	<i>c_{verysh.}</i>	<i>RMSE</i>	<i>R²</i>	<i>PSE</i>
		[-]	[-]	[-]	[-]	[-]	[-]	[-]	[-]	[-]	[-]	[-]	[-]	[-]	[-]	[-]	[-]
Mod. VDM (2003)	Plunging	9.37	0.48	0.83	0.23	9.43	0.31	0.91	0.10	9.35	0.53	0.88	0.31	Nan	0.84	0.74	1.27
	Surging	1.40				1.36				1.40				0.98			
Simple van Gent (2003)		1.79	0.45	0.75	0.20	1.79	0.41	0.69	0.17	1.85	0.63	0.71	0.42	1.56	0.29	0.94	0.12
MK (2011)	Plunging	5.06				5.16				4.56				Nan			
	Surging	4.87	0.63	0.80	0.40	4.92	0.60	0.75	0.37	4.59	0.52	0.93	0.28	4.17	0.40	0.96	0.26
EA (2019)	Plunging	4.58				4.48				4.85				Nan			
	Surging	3.33	0.26	0.91	0.07	3.19	0.22	0.92	0.05	3.64	0.34	0.90	0.12	3.33	0.22	0.96	0.07
ES (2020)	Plunging	5.03				5.07				5.17				Nan			
	Surging	4.29	0.32	0.87	0.10	4.12	0.27	0.87	0.07	4.86	0.44	0.86	0.21	6.56	0.33	0.93	0.20
Rwr. VDM (2021)	Plunging	6.90				6.77				7.15				Nan			
	Surging	1.01	0.33	0.86	0.11	0.98	0.24	0.89	0.06	1.18	0.36	0.89	0.14	0.83	0.82	0.43	1.08
Mod. van Gent (2025)		2.63	0.35	0.84	0.12	2.58	0.32	0.82	0.10	2.73	0.47	0.82	0.23	3.06	0.21	0.96	0.07
		<i>c_{new}</i>	μ	<i>Std</i>	<i>CoV</i>	<i>c_{deep}</i>	μ	<i>Std</i>	<i>CoV</i>	<i>c_{shallow}</i>	μ	<i>Std</i>	<i>CoV</i>	<i>c_{verysh.}</i>	μ	<i>Std</i>	<i>CoV</i>
		[-]	[%]	[-]	[%]	[-]	[%]	[-]	[%]	[-]	[%]	[-]	[%]	[-]	[%]	[-]	[%]
Mod. VDM (2003)	Plunging	9.37	-5.89	0.45	149	9.43	-3.88	0.29	126	9.35	-6.20	0.50	112	Nan	-16.51	0.74	119
	Surging	1.40				1.36				1.40				0.98			
Simple van Gent (2003)		1.79	-8.58	0.41	118	1.79	-8.17	0.38	120	1.85	-12.59	0.55	103	1.56	-4.10	0.28	114
MK (2011)	Plunging	5.06				5.16				4.56				Nan			
	Surging	4.87	-6.11	0.58	124	4.92	-5.54	0.56	128	4.59	-4.66	0.47	111	4.17	0.01	0.41	149
EA (2019)	Plunging	4.58				4.48				4.85				Nan			
	Surging	3.33	-4.73	0.24	119	3.19	-3.58	0.20	126	3.64	-4.59	0.33	122	3.33	-0.60	0.23	148
ES (2020)	Plunging	5.03				5.07				5.17				Nan			
	Surging	4.29	-6.02	0.29	115	4.12	-6.80	0.23	108	4.86	-9.33	0.38	100	6.56	-8.13	0.30	114
Rwr. VDM (2021)	Plunging	6.90				6.77				7.15				Nan			
	Surging	1.01	-5.72	0.31	138	0.98	-6.54	0.20	107	1.18	-4.10	0.35	124	0.83	-29.78	0.57	88
Mod. van Gent (2025)		2.63	-5.63	0.33	123	2.58	-5.04	0.30	128	2.73	-5.80	0.44	114	3.06	-4.38	0.20	112

Data availability

Data will be made available on request.

References

Bali, M., Etemad-Shahidi, A., van Gent, M.R.A., 2023. On the stability of rubble mound structures under oblique wave attack. *J. Mar. Sci. Eng.* 11 (7), 1261. <https://doi.org/10.3390/jmse11071261>.

Battjes, J., 1974. Surf similarity. In: *Coastal Engineering Proceedings 1974*, pp. 466–480. <https://doi.org/10.1061/9780872621138.029>.

Battjes, J.A., Groenendijk, H.W., 2000. Wave height distributions on shallow foreshores. *Coast. Eng.* 40, 161–182. [https://doi.org/10.1016/S0378-3839\(00\)00007-7](https://doi.org/10.1016/S0378-3839(00)00007-7).

Booij, N., Ris, R.C., Holthuijsen, L.H., 1999. A third-generation wave model for coastal regions: 1. Model description and validation. *J. Geophys. Res.: Oceans (San Franc.)* 104 (C4), 7649–7666. <https://doi.org/10.1029/98JC02622>.

Burcharth, H.F., Andersen, T.L., Medina, J.R., 2010. Stability of cubipod armoured roundheads in short-crested waves. A comparison between cubipod and cube armour stability. *Coastal Engineering Proceedings* 1 (32), 1–10. <https://doi.org/10.9753/icce.v32.structures.39>.

CIRIA/CUR/CETMEF, 2007. *The rock manual. The Use of Rock in Hydraulic Engineering*. CIRIA.

de Ridder, M.P., van Kester, D.C.P., van Bentem, R., Teng, D.Y.Y., van Gent, M.R.A., 2024. Wave overtopping discharges at rubble mound structures in shallow water. *Coast. Eng.* 194, 104626. <https://doi.org/10.1016/j.coastaleng.2024.104626>.

Eldrup, M.R., Andersen, T.L., 2019. Extension of shallow water rock armour stability formulae to nonlinear waves. *Coast. Eng.* 153, 103536. <https://doi.org/10.1016/j.coastaleng.2019.103536>.

Eldrup, M.R., Lykke Andersen, T., Burcharth, H.F., 2019. Stability of rubble mound breakwaters—a study of the notional permeability factor, based on physical model tests. *Water (Lond. 1974)* 11 (5), 934. <https://doi.org/10.3390/w11050934>.

Etemad-Shahidi, A., Bali, M., van Gent, M.R.A., 2020. On the stability of rock armoured rubble mound structures. *Coast. Eng.* 158, 103655. <https://doi.org/10.1016/j.coastaleng.2020.103655>.

Goda, Y., 2010. *Random seas and design of maritime structures*. World scientific.

Goda, Y., 2012. Design wave height selection in intermediate-depth waters. *Coast. Eng.* 66, 3–7. <https://doi.org/10.1016/j.coastaleng.2012.03.005>.

Herrera, M.P., Gomez-Martín, M.E., Medina, J.R., 2017. Hydraulic stability of rock armors in breaking wave conditions. *Coast. Eng.* 127, 55–67. <https://doi.org/10.1016/j.coastaleng.2017.06.010>.

Hofland, B., Chen, X., Altomare, C., Oosterlo, P., 2017. Prediction formula for the spectral wave period $T_{m-1.0}$ on mildly sloping shallow foreshores. *Coast. Eng.* 123, 21–28. <https://doi.org/10.1016/j.coastaleng.2017.02.005>.

Hudson, R.Y., 1959. Laboratory investigation of rubble-mound breakwaters. *J. Waterw. Harb. Div.* 85 (3), 93–121.

Hughes, S.A., 2004. Wave momentum flux parameter: a descriptor for nearshore waves. *Coast. Eng.* 51 (11–12). <https://doi.org/10.1016/j.coastaleng.2004.07.025>, 1067–1084; 1067–84.

Iribarren, R., 1938. Una Fórmula para el Cálculo de los Diques de Escollera.

Jumelet, D., van Gent, M.R.A., Hofland, B., Kuiper, C., 2023. Stability of rock-armoured mild slopes. *Coast. Eng.* 187, 104418. <https://doi.org/10.1016/j.coastaleng.2023.104418>.

Kroon, A., de Schipper, M.A., van Gelder, P.H.A.J.M., Aarninkhof, S.G.J., 2020. Ranking uncertainty: wave climate variability versus model uncertainty in probabilistic assessment of coastline change. *Coast. Eng.* 158, 103673. <https://doi.org/10.1016/j.coastaleng.2020.103673>.

Lee, A., Geem, Z.W., Suh, K.-D., 2016. Determination of optimal initial weights of an artificial neural network by using the harmony search algorithm: application to breaker armor stones. *Appl. Sci.* 6 (6), 164. <https://doi.org/10.3390/app6060164>.

Lee, J.-S., Suh, K.-D., 2020. Development of stability formulas for rock armor and tetrapods using multigene genetic programming. *J. Waterw. Port, Coast. Ocean Eng.* 146 (1), 04019027. [https://doi.org/10.1061/\(ASCE\)WW.1943-5460.0000540](https://doi.org/10.1061/(ASCE)WW.1943-5460.0000540).

Losada, M.A., 2021. Method to assess the interplay of slope, relative water depth, wave steepness, and sea state persistence in the progression of damage to the rock layer over impermeable dikes. *Ocean Eng.* 239, 109904. <https://doi.org/10.1016/j.oceaneng.2021.109904>.

Losada, M.A., Gimenez-Curto, L.A., 1979. The joint effect of the wave height and period on the stability of rubble mound breakwaters using Iribarren's number. *Coast. Eng.* 3, 77–96. [https://doi.org/10.1016/0378-3839\(79\)90011-5](https://doi.org/10.1016/0378-3839(79)90011-5).

Maciñeira, E.G., Burcharth, H.F., 2016. Stability of cube armoured roundheads exposed to long crested and short crested waves. *Coast. Eng.* 112, 99–112. <https://doi.org/10.1016/j.coastaleng.2016.03.002>.

Mares-Nasarre, P., Molines, J., Gómez-Martín, M.E., Medina, J.R., 2021. Explicit Neural Network-derived formula for overtopping flow on mound breakwaters in depth-limited breaking wave conditions. *Coast. Eng.* 164, 103810. <https://doi.org/10.1016/j.coastaleng.2020.103810>.

Mares-Nasarre, P., van Gent, M.R.A., Morales-Nápoles, O., 2024. A copula-based model to describe the uncertainty of overtopping variables on mound breakwaters. *Coast. Eng.* 189, 104483. <https://doi.org/10.1016/j.coastaleng.2024.104483>.

Marino, S., Scaravaglione, G., Francione, A., Valentini, N., Saponieri, A., Damiani, L., van Gent, M.R.A., Tomasichio, G., 2022. Laboratory investigation on armour stability for extremely shallow water conditions. In: *Proceedings of the IAHR World Congress. Proceedings of the 39th IAHR World Congress*, pp. 5973–5979. <https://doi.org/10.3850/iahr-39wc2521711920221364>. Code 299039, 2022.

- Mase, H., Sakamoto, M., Sakai, T., 1995. Neural network for stability analysis of rubble-mound breakwaters. *J. Waterw. Port, Coast. Ocean Eng.* 121 (6), 294–299. [https://doi.org/10.1061/\(ASCE\)0733-950X\(1995\)121:6\(294\)](https://doi.org/10.1061/(ASCE)0733-950X(1995)121:6(294)).
- Melby, J.A., Hughes, S.A., 2003. Armor stability based on wave momentum flux. *Coastal Structures* 2003. [https://doi.org/10.1061/40733\(147\)5](https://doi.org/10.1061/40733(147)5). Reston, vol. A.
- Melby, J.A., Kobayashi, N., 2011. Stone armor damage initiation and progression based on the maximum wave momentum flux. *J. Coast Res.* 27 (1), 110–119. <https://doi.org/10.2112/JCOASTRES-D-09-00122.1>.
- Medina, J.R., González-Escrivá, J.A., Garrido, J., De Rouck, J., 2003. Overtopping analysis using neural networks. *Coast. Eng.* 2002, 2165–2177. https://doi.org/10.1142/9789812791306_0182.
- Scaravaglione, G., Marino, S., Francone, A., Damiani, L., Tomasicchio, G.R., Saponieri, A., 2024. Laboratory investigation on pore pressures inside a rubble mound breakwater in depth-limited waters. *Appl. Ocean Res.* 147, 103988. <https://doi.org/10.1016/j.apor.2024.103988>.
- Scaravaglione, G., Marino, S., Francone, A., Leone, E., Damiani, L., Tomasicchio, G.R., van Gent, R.M.A., Saponieri, A., 2025. The influence of shallow water on rock armour stability. *Coast. Eng.* 197, 104657. <https://doi.org/10.1016/j.coastaleng.2024.104657>.
- Smith, G., Wallast, L., van Gent, M.R.A., 2002. Rock slope stability with shallow foreshores. In: *Coastal Engineering Proceedings 2002*. https://doi.org/10.1142/9789812791306_0128.
- Thompson, D.M., Shuttler, R.M., 1975. *Riprap Design for Wind-Wave Attack, a Laboratory Study in Random Waves*. Wallingford report EX707 for CIRIA, H. R. Wallingford.
- USACE, 2002. CEM: Coastal Engineering Manual. U.S. Army Corps of Engineers. http://books.google.com/books?id=QLO_jwEACAAJ.
- Van der Meer, J.W., 1988. *Rock Slopes and Gravel Beaches under Wave Attack*. Ph.D. Thesis, Delft Hydraulics.
- Van der Meer, J.W., 2021. Rock armour slope stability under wave attack; the Van der Meer Formula revisited. *Journal of Coastal and Hydraulic Structures* 1. <https://doi.org/10.48438/jchs.2021.0008>.
- Van der Meer, J.W., Lykke Andersen, T., Eldrup, M.R., 2024. Rock armour slope stability under wave attack in shallow water. *Journal of Coastal and Hydraulic Structures* 4. <https://doi.org/10.59490/jchs.2024.0035>.
- Van Gent, M.R.A., 2001. Wave runup on dikes with shallow foreshores. *J. Waterw. Port, Coast. Ocean Eng.* 127 (5), 254–262. [https://doi.org/10.1061/\(ASCE\)0733-950X\(2001\)127:5\(254\)](https://doi.org/10.1061/(ASCE)0733-950X(2001)127:5(254)).
- Van Gent, M.R.A., 2004. On the stability of rock slopes. Environmentally friendly coastal protection: proceedings of the NATO advanced research workshop on environmentally friendly coastal protection structures varna, Bulgaria. https://doi.org/10.1007/1-4020-3301-X_5.
- Van Gent, M.R.A., Smale, A.J., Kuiper, C., 2003. Stability of rock slopes with shallow foreshores. *Coastal Structures* 2003. [https://doi.org/10.1061/40733\(147\)9](https://doi.org/10.1061/40733(147)9).
- Van Gent, M.R.A., 1999. Physical model investigations on coastal structures with shallow foreshores: 2D model tests with single and double-peaked wave energy spectra. <http://doi.org/10.13140/RG.2.2.17091.68644>.
- Van Gent, M.R.A., Wolters, G., 2018. Effects of storm duration and oblique wave attack on open filters underneath rock armoured slopes. *Coast. Eng.* 135, 55–65. <https://doi.org/10.1016/j.coastaleng.2018.01.009>.
- Verhagen, H.J., Mertens, M., 2009. Riprap stability for deep water, shallow water and steep foreshores. In: *Coasts, Marine Structures and Breakwaters: Adapting To Change: Proceedings Of the 9th International Conference Organised by the Institution Of Civil Engineers* 486–95. Thomas Telford Ltd, Edinburgh. <https://doi.org/10.1680/cmsb.41318.0046>.
- Vidal, C., Medina, R., Lomónaco, P., 2006. Wave height parameter for damage description of rubble-mound breakwaters. *Coast. Eng.* 53 (9), 711–722. <https://doi.org/10.1016/j.coastaleng.2006.02.007>.
- Wei, X., Liu, H., She, X., Lu, Y., Liu, X., Mo, S., 2019. Stability assessment of rubble mound breakwaters using extreme learning machine models. *J. Mar. Sci. Eng.* 7 (9), 312. <https://doi.org/10.3390/jmse7090312>.

Abbreviation

- Confidence level: CL
 Double peaked spectrum: DOUBLE
 Eldrup and Andersen: EA
 Etemad-Shahidi et al: ES
 EUropean Maritime & Environmental Research: EUMER
 Infragravity waves: IG
 Interquartile range method: IQR
 Melby and Kobayashi: MK

- Pierson-Moskowitz: PM
 Surf Similarity Parameter: SSP
 Thompson and Shuttler: TS
 Texel-Marsen-Arsloe: TMA
 Van der Meer: VDM
 Vidal, Medina and Lomónaco: VML
 Van Gent, Smale and Kuiper: VSK

Glossary

- Structure seaward slope angle: α [°]
 Foreshore slope angle: β [°]
 Relative buoyant density of the rock armour: Δ [-]
 Relative Bias: μ [%]
 Surf similarity parameter using H_{m0} and $T_{m-1,0}$: $\xi_{m-1,0}$ [-]
 Transition surf similarity parameter in EA equation: $\xi_{m-1,0,c}$ [-]
 Surf similarity parameter using H_s and $T_{m-1,0}$: $\xi_{s-1,0}$ [-]
 Transition surf similarity parameter in Rewritten VDM equation: $\xi_{s-1,0,c}$ [-]
 Nonlinearity parameter: I_0 [-]
 Density of the armor rock: ρ_r [Kg/m³]
 Density of the water: ρ_w [Kg/m³]
 Eroded area: A_e [m²]
 Coefficients in Hughes equation: A_0, A_1 [-]
 Berm width: B [-]
 Blockiness coefficient: BLc [%]
 Regression fitting coefficients for the stability equations: c [-]
 Coefficient of Variation: CoV [%]
 Stone shape coefficients: c_{pb}, c_{su} [-]
 Permeability coefficient, $C_p = \left[1 + \left(\frac{D_{n50,core}}{D_{n50}} \right)^{3/10} \right]^{3/5} : C_p$ [-]
 Armor nominal median stone diameter, $D_{n50} = (M_{50}/\rho_r)^{1/3} : D_{n50}$ [m]
 Core nominal median stone diameter: $D_{n50,core}$ [m]
 Grading uniformity coefficient: D_{85}/D_{15} [-]
 Mass exceeded by 85% of a sample by weight: D_{85} [m]
 Mass exceeded by 15% of a sample by weight: D_{15} [m]
 Gravity acceleration: g [m/s²]
 Water depth at toe of the structure: h [m]
 Dimensionless depth, $\tilde{h} = \frac{h}{H_{m0,deep}} \left(\frac{cot \beta}{100} \right)^{0.2} : \tilde{h}$ [-]
 Relative water depth, $h_r = H_{m0,deep}/h : h_r$ [-]
 Significant wave height in the time domain, $H_s = H_{1/3} : H_s$ [m]
 Significant (spectral) wave height in frequency domain, $H_{m0} = 4(m_0)^{1/2} : H_{m0}$ [m]
 Wave height exceeded by 2 percent of the waves in time domain: $H_2\%$ [m]
 Wavelength using T_m : L_m [m]
 Wavelength using $T_{m-1,0}$: $L_{m-1,0}$ [m]
 Length-to-thickness ratio: LT [-]
 Foreshore slope, $m = \tan \beta : m$ [-]
 Total number of observations in error metrics evaluation: M [-]
 Nonlinear maximum wave momentum flux: $(M_f)_{max}$ [N/m]
 Mean squared error: MSE [-]
 Median mass of the armor rock grading: M_{50} [Kg]
 Number of tests: N [-]
 Stability number in the MK equation: N_m [-]
 Stability number: N_s [-]
 Number of waves: N_w [-]
 Number of explanatory variables in the model: p [-]
 Notional permeability factor: P [-]
 Predicted squared error: PSE [-]
 Root Mean Square Error: $RMSE$ [-]
 Determination coefficient: R^2 [-]
 Damage level: S [-]
 Damage design value: S_d [-]
 Damage best estimate: $S_{best-estimate}$ [-]
 Wave steepness using H_{m0} and T_m : s_m [-]
 Transition wave steepness in MK equation: $s_{m,c}$ [-]
 Wave steepness using H_{m0} and $T_{m-1,0}$: $s_{m-1,0}$ [-]
 Standard Deviation: Std [-]
 Negative spectral energy wave period, $T_{m-1,0} = m_{-1}/m_0 : T_{m-1,0}$ [s]
 Mean period in the time domain: T_m [s]